

Structure-Preserving Reduced-Order Modeling via Low-Rank Transport Signatures

Jiajia Yu* Jingwei Hu[†] Fengyan Li[‡] Shanyin Tong[§]
 Yunan Yang[¶] Zhaiming Shen^{||}

Abstract

Parametrized PDEs with density-valued solutions are often difficult to approximate with classical linear reduced-order models, especially in transport-dominated regimes. We introduce an optimal-transport-based reduced-order modeling that represents each density by the Kantorovich potential transporting a fixed reference density to the target density, and then maps these potentials to transport signatures using a weighted Laplacian associated with the reference measure. This embeds the density-valued solution map in a Hilbert space while preserving control of the induced transport maps and Wasserstein error. We treat the signature map as a continuous matrix indexed by parameters and space, construct a low-rank skeleton decomposition using a maximal-volume criterion, and learn the parameter-to-coefficient map with a neural network for efficient non-intrusive online evaluation. The reconstructed solution is obtained by pushing forward the reference density, so mass preservation is built into the method. We prove a mean-squared Wasserstein error bound separating low-rank approximation, discretization, sampling, and learning errors, and demonstrate the method on a two-dimensional continuity equation, where transport signatures yield substantially lower-rank structure than the original density snapshots.

1 Introduction

Parametrized partial differential equations arise in many-query and real-time settings where a high-fidelity model must be evaluated repeatedly for many parameter values. Reduced-order modeling (ROM) seeks to replace such high-dimensional simulations by inexpensive surrogate models that retain the dominant dependence of the solution on the parameters. Classical approaches, including proper orthogonal decomposition (POD) and reduced-basis

*jiajia.yu@duke.edu. Department of Mathematics, Duke University, Durham, NC 27710

[†]hujw@uw.edu. Department of Applied Mathematics, University of Washington, Seattle, WA 98195

[‡]lif@rpi.edu. Department of Mathematical Sciences, Rensselaer Polytechnic Institute, Troy, NY 12180

[§]tong3@sas.upenn.edu. Department of Mathematics, University of Pennsylvania, Philadelphia, PA 19104

[¶]yunan.yang@cornell.edu. Department of Mathematics, Cornell University, Ithaca, NY 14850

^{||}zshen49@gatech.edu. School of Mathematics, Georgia Institute of Technology, Atlanta, GA 30332

methods, construct a low-dimensional linear approximation space from representative snapshots and then approximate new solutions by projection or regression in this space [4, 16, 18]. These methods have been highly successful for many elliptic, parabolic, and mildly nonlinear problems, especially when the associated solution manifold has rapidly decaying Kolmogorov widths [9, 12, 17, 26].

However, transport-dominated problems pose a persistent challenge for linear reduced-order models. When coherent structures translate, deform, or concentrate, the solution manifold may be intrinsically low-dimensional but poorly approximated by a fixed linear subspace. A simple traveling wave, for instance, can require many linear modes despite being described by only a few physical parameters. This phenomenon is often referred to as the Kolmogorov-width barrier for transport-dominated problems. It has motivated a broad class of nonlinear ROM techniques, including shifted bases, registration methods, Lagrangian formulations, transported subspaces, adaptive bases, and neural-network-based nonlinear manifolds [6, 25, 28].

The difficulty is even more pronounced when the state variable is a probability distribution or density. Linear combinations of density snapshots can destroy positivity, distort mass, and measure error in a geometry that is insensitive to displacement. For density-valued PDEs, such as continuity equations and Fokker–Planck equations, it is natural to compare solutions by the cost of transporting mass rather than by pointwise amplitude differences. Optimal transport provides precisely such a geometry through the Wasserstein distance, and it has become a central tool in the analysis and computation of probability measures [20, 27, 29, 31].

Several reduced-order modeling strategies have recently incorporated ideas from optimal transport. One line of work formulates model reduction directly in metric or Wasserstein spaces, using Wasserstein barycenters or tangent-space approximations to construct nonlinear reduced models for families of probability measures [3, 11]. A related approach uses sparse Wasserstein barycenters to approximate and interpolate parametrized families of measures [10]. Optimal transport has also been combined with classical reduced-order modeling techniques, for example through POD-based approximations for kinetic equations [5]. Another line of work uses displacement interpolation to generate physically meaningful interpolants between density snapshots or to augment limited training data [21]. Optimal-transport-based registration methods have been used to align moving features before applying classical reduced-basis approximation [6]. More broadly, linearized optimal transport and Monge-type embeddings provide Hilbert-space representations of probability measures through optimal maps from a reference distribution [22–24, 32]. These works demonstrate that optimal transport can overcome some limitations of linear ROMs for transport-dominated data, while preserving important geometric and physical structure.

In this paper, we introduce an optimal-transport-based reduced-order modeling framework for probability distributions generated by parametrized partial differential equations. Let $\rho(\mu)$ denote the probability distribution associated with parameter value μ , where time may be included among the parameters. Instead of constructing a reduced-order model directly for the densities $\rho(\mu)$, we first represent each distribution by the Kantorovich potential $\phi(\mu)$ transporting a fixed reference distribution $\bar{\rho}$ to $\rho(\mu)$. Thus the corresponding optimal transport map is

$$T_{\bar{\rho} \rightarrow \rho(\mu)} = I - \nabla \phi(\mu).$$

We then define a transport signature

$$\Psi(\mu, \cdot) = (I - \mathcal{L})^{1/2} \phi(\mu),$$

where $\mathcal{L} = \nabla \cdot (\bar{\rho} \nabla)$ is a weighted Laplacian associated with the reference distribution. This transformation places the family of transport potentials in a Hilbert-space setting while retaining direct control of the transport maps: approximation error in the signature controls the $L^2(\bar{\rho})$ error of the corresponding optimal maps, and hence controls the induced 2-Wasserstein error after pushforward.

The central computational idea is to regard $\Psi(\mu, x)$ as a continuous matrix, or cmatrix, with rows indexed by the parameter μ and columns indexed by the spatial variable x [30]. We then construct a low-rank approximation in this transport-signature space using a skeleton decomposition based on a maximal volume criterion [13–15]. The selected rows correspond to transport signatures at representative parameter values,

$$\psi_s(\cdot) = \Psi(\mu_{i_s}, \cdot), \quad s = 1, \dots, r.$$

For each training parameter μ_j , we compute coefficients by least-squares fitting on a spatial grid with m points, obtaining an approximation of the form

$$\Psi(\mu_j, x) \approx \sum_{s=1}^r a_{m,s}(\mu_j) \psi_s(x).$$

A neural network is then trained to learn the parameter-to-coefficient map

$$\mu \mapsto a_m(\mu).$$

For a new parameter value μ , the online stage evaluates the learned coefficients, reconstructs the transport signature, maps it back to an approximate potential, differentiates to obtain an approximate transport map, and finally pushes forward the reference distribution:

$$\hat{\rho}_{n,m}^r(\mu) = (\hat{\mathbf{T}}_{n,m}^r(\mu, \cdot))_{\#} \bar{\rho}.$$

Thus the final output is again a probability distribution, with mass preservation built into the reconstruction.

The proposed method differs from existing optimal-transport ROMs in several respects. Wasserstein barycenter approaches typically require the solution of a barycenter problem over a dictionary of measures during reconstruction, whereas our online stage only evaluates a learned coefficient map and pushes forward the reference distribution. Displacement interpolation methods construct approximations along Wasserstein geodesics between selected snapshots. In contrast, our method builds a global reduced representation in transport-signature space. Similarly, instead of using optimal transport only as a registration or alignment step before applying a classical reduced-basis method, we construct the reduced order model directly from transport signatures associated with the density-valued solution map. The resulting skeleton decomposition selects representative signatures and yields an interpretable low-rank structure, while the learned parameter-to-coefficient map provides a non-intrusive online evaluation procedure.

Our main theoretical result gives a mean-squared W_2 error bound for the reconstructed distribution $\widehat{\rho}_{n,m}^r(\mu)$ relative to the true distribution $\rho(\mu)$. The bound separates the principal sources of error: the low-rank approximation error in transport-signature space, the effect of spatial discretization and quadrature, the coverage of the parameter samples, and the statistical error from learning the coefficient map. This analysis connects approximation in the Hilbert space of signatures to error in the natural Wasserstein geometry of probability distributions.

We demonstrate the framework on the density-valued continuity equation in two spatial dimensions. The results show that transport signatures can exhibit substantially more favorable low-rank structure than the original density snapshots, leading to accurate reduced-order approximations with a small number of selected transport-based basis.

The rest of the paper is organized as follows. Section 2 reviews the background material needed for the proposed ROM method, including optimal transport theory, computational aspects of optimal transport, and the skeleton decomposition algorithm. Section 3 presents the transport-signature-based ROM method, and Section 4 provides a rigorous theoretical error analysis. Numerical examples are given in Section 5, followed by concluding remarks in Section 6.

2 Background

This section provides essential background for the proposed optimal transport-based reduced-order method.

2.1 Optimal transport

Let Ω be a subset of the Euclidean space and $\mathbb{P}(\Omega)$ be the set of probability distributions on Ω . For given $\rho_0, \rho_1 \in \mathbb{P}(\Omega)$, the goal of optimal transport is to find the map that moves ρ_0 to ρ_1 with the least effort. Given a cost function $c : \Omega \times \Omega \rightarrow \mathbb{R}$, the Monge problem seeks a measurable map $T : \Omega \rightarrow \Omega$ solving

$$\inf_T \left\{ \int_{\Omega} c(x, T(x)) d\rho_0(x) : T_{\#}\rho_0 = \rho_1 \right\}, \quad (1)$$

where $T_{\#}\rho_0$ denotes the push-forward measure of ρ_0 by T . More precisely,

$$(T_{\#}\rho_0)(B) = \rho_0(T^{-1}(B)) \quad \text{for any measurable } B \subset \Omega \quad (2)$$

A minimizer of (1), when it exists, is called an *optimal transport map*.

Potentials and transport signature Since the Monge problem imposes that mass moves deterministically through a map, an optimal transport map may fail to exist in general. A relaxation is the Kantorovich problem optimizing over transport plans:

$$\inf_{\pi \in \Pi(\rho_0, \rho_1)} \int_{\Omega \times \Omega} c(x, y) d\pi(x, y). \quad (3)$$

Here, $\Pi(\rho_0, \rho_1)$ denotes the set of probability measures on $\Omega \times \Omega$ whose marginals are ρ_0 and ρ_1 . The Kantorovich formulation gives rise to the *p-Wasserstein distance*

$$W_p(\rho_0, \rho_1) := \left(\inf_{\pi \in \Pi(\rho_0, \rho_1)} \int_{\Omega \times \Omega} \|x - y\|_p^p d\pi(x, y) \right)^{1/p}. \quad (4)$$

For the quadratic cost $c(x, y) = \frac{1}{2}\|x - y\|_2^2$, the Kantorovich problem (3) has the following equivalent dual formulation:

$$\sup_{\phi, \eta} \left\{ \int_{\Omega} \phi(x) d\rho_0(x) + \int_{\Omega} \eta(y) d\rho_1(y) : \phi(x) + \eta(y) \leq \frac{1}{2}\|x - y\|_2^2 \right\}. \quad (5)$$

The maximizers ϕ and η , when they exist, are called *Kantorovich potentials*.

Let $\mathbb{P}_2(\mathbb{R}^d)$ be the set of probability distributions with finite second moment. A fundamental result in optimal transport ([29, Thm. 1.22] [7]) shows that, for the quadratic cost, the optimal transport map exists and is induced by a convex potential function.

Theorem 1 (Brenier Theorem). *Let $\rho_0, \rho_1 \in \mathbb{P}_2(\mathbb{R}^d)$ and assume that $\rho_0 \ll dx$. For the quadratic cost $c(x, y) = \frac{1}{2}\|x - y\|_2^2$, there exists a ρ_0 -a.e. unique optimal transport map T pushing ρ_0 forward to ρ_1 . Moreover, there exists a convex function $u : \mathbb{R}^d \rightarrow \mathbb{R}$, unique up to an additive constant, such that*

$$T = \nabla u, \quad \rho_0\text{-a.e.}$$

The convex function u is often called the *optimal transport potential*, also known as the *Brenier potential*. In particular, u is associated with the Kantorovich potential ϕ under the assumptions of Brenier's theorem (Theorem 1) via

$$u(x) = \frac{1}{2}\|x\|_2^2 - \phi(x). \quad (6)$$

Let $(\mathbb{P}_2(\mathbb{R}^d), W_2)$ denote the Wasserstein-2 space. At an absolutely continuous measure $\bar{\rho}$, one can define the tangent cone to $\bar{\rho}$ in $(\mathbb{P}_2(\mathbb{R}^d), W_2)$ using optimal transport maps following [2, Eq. 8.5.1].

$$\text{Tan}_{\bar{\rho}} \mathbb{P}_2(\mathbb{R}^d) := \overline{\{\lambda(T - I) : T \text{ is the optimal transport map from } \bar{\rho} \text{ to } T_{\#}\bar{\rho}, \lambda > 0\}}^{L^2(\bar{\rho}; \mathbb{R}^d)} \quad (7)$$

According to [2, Thm. 8.5.1], the tangent cone is in fact a linear subspace of $L^2(\bar{\rho}; \mathbb{R}^d)$:

$$\text{Tan}_{\bar{\rho}} \mathbb{P}_2(\mathbb{R}^d) = \overline{\{\nabla \varphi : \varphi \in C_c^\infty(\mathbb{R}^d)\}}^{L^2(\bar{\rho}; \mathbb{R}^d)}. \quad (8)$$

This characterization motivates the construction of a reduced-order model in the tangent space. Since the optimal transport displacement satisfies $T - I = -\nabla \phi$, where ϕ is a Kantorovich potential, the transport information is encoded in ϕ . We therefore use Kantorovich potentials to derive transport signatures and construct the reduced-order model.

Computation: the back-and-forth method In this work, we also compute the optimal transport map using the back-and-forth method of [19] when the PDE solution is dimension bigger than one. It is based on the Kantorovich dual formulation (5).

Define the c -transform of ϕ and η as

$$\phi^c(y) := \inf_{x \in \Omega} \{c(x, y) - \phi(x)\}, \quad \eta^c(x) := \inf_{y \in \Omega} \{c(x, y) - \eta(y)\}, \quad (9)$$

Instead of optimizing over all pairs (ϕ, η) satisfying the inequality constraint, one can optimize over a single potential at a time: if η is fixed, then the best admissible choice of ϕ is $\phi = \eta^c$, and vice versa. More concretely, define the reduced dual objectives

$$\mathcal{I}(\phi) := \int_{\Omega} \phi(x) d\rho_0(x) + \int_{\Omega} \phi^c(y) d\rho_1(y), \quad \mathcal{J}(\eta) := \int_{\Omega} \eta^c(x) d\rho_0(x) + \int_{\Omega} \eta(y) d\rho_1(y). \quad (10)$$

The method moves “back and forth” between the two dual variables, using the c -transform to maintain admissibility while using gradient ascent to increase the dual objective. Given a step size $\sigma > 0$, one iteration has the form

$$\phi_{n+\frac{1}{2}} = \phi_n + \sigma \nabla_{\dot{H}^1} \mathcal{I}(\phi_n), \quad \eta_{n+\frac{1}{2}} = \phi_{n+\frac{1}{2}}^c, \quad (11)$$

$$\eta_{n+1} = \eta_{n+\frac{1}{2}} + \sigma \nabla_{\dot{H}^1} \mathcal{J}(\eta_{n+\frac{1}{2}}), \quad \phi_{n+1} = \eta_{n+1}^c. \quad (12)$$

Denote $T_\phi = I - \nabla \phi^c$ and $T_\eta = I - \nabla \eta^c$, the homogeneous \dot{H}^1 gradients are computed by

$$\nabla_{\dot{H}^1} \mathcal{I}(\phi) = (-\Delta)^{-1} (\rho_0 - (T_\phi)_\# \rho_1), \quad \nabla_{\dot{H}^1} \mathcal{J}(\eta) = (-\Delta)^{-1} (\rho_1 - (T_\eta)_\# \rho_0). \quad (13)$$

The update increases the potential in regions where the current map transports too little mass and decreases it where too much mass is transported. The inverse Laplacian acts as a preconditioner, producing a smooth correction to the potential.

From a computational point of view, the method is efficient on regular grids. Each iteration requires two main operations: computing c -transforms and solving Poisson-type equations arising from the \dot{H}^1 gradient. For quadratic costs on grid-based discretizations, the c -transforms can be computed in nearly linear time, while the inverse Laplacian can be applied efficiently using fast Fourier transforms or related elliptic solvers. As a result, for m grid points, the method has approximately $O(m \log m)$ computational cost per iteration and $O(m)$ memory usage. This makes the back-and-forth method suitable for large-scale problems where one needs not only the Wasserstein distance but also an accurate approximation of the optimal transport map T .

2.2 Skeleton decomposition

Next, let us introduce the skeleton decomposition. Given a matrix $A \in \mathbb{R}^{m \times n}$, letting $I = \{i_1, \dots, i_r\}$ and $J = \{j_1, \dots, j_r\}$ be the row and column indices, we denote by $A_{I,:}$ all the rows of A with row indices in I and $A_{:,J}$ the all the columns of A with column indices in J . Assume that the submatrix $A_{I,J}$ situated on rows I and columns J is nonsingular. Then

$$A_{:,J} A_{I,J}^{-1} A_{I,:} \approx A \quad (14)$$

is called a matrix skeleton or cross approximation [13–15]. Note that the left-hand side of (14) is also called CUR decomposition in the literature. One notable advantage of skeleton decomposition over classical SVD is interpretability. While SVD expresses data in an abstract basis (e.g., eigenspaces), obscuring the physical meaning of the original rows and columns, skeleton decomposition retains actual rows and columns of the matrix, preserving their physical interpretation. Additionally, SVD becomes computationally prohibitive for large-scale problems, whereas skeleton decomposition offers a more scalable alternative.

More recently, it is shown in [1] that when $A_{I,J}$ has the maximal volume (absolute value of the determinant) among all $r \times r$ submatrices of A , then the Chebyshev (maximum) norm of the residual matrix satisfies

$$\|A - A_{:,J}A_{I,J}^{-1}A_{I,:}\|_C \leq \frac{r+1}{\sqrt{\sum_{k=1}^{r+1} \sigma_k^{-2}(A)}}, \quad (15)$$

where $\sigma_k(A)$ is the k -th singular value of A .

Algorithmically, a greedy-based iterative approach was proposed in [1] to effectively select the rows and columns based on the maximal volume criterion. We summarize it in Algorithm 1.

For our purpose, it suffices to select indices along only one direction (either rows or columns, as will be explained in Section 3). We therefore specialize Algorithm 1 to the symmetric matrix setting, where the same indices are selected for both rows and columns. The new procedure for selecting symmetric indices based on the maximal volume criterion is summarized in Algorithm 2.

Algorithm 1 Skeleton Decomposition via Maximal Volume

Require: $n \times m$ matrix M , $r \times r$ submatrix A_0 with $\det(A_0) \neq 0$, tolerance $\epsilon > 0$, $l = 0$, $b_{ij} = \infty$ and $A_l = A_0$

Ensure: A_l a close to dominant submatrix with indices (I_l, J_l) in M

- 1: **while** $|b_{ij}| > 1 + \epsilon$ **do**
 - 2: Let $B_l = M(:, J_l)A_l^{-1}$, and $C_l = A_l^{-1}M(I_l, :)$
 - 3: Set b_{ij} equal to the largest in modulus entry of both B_l and C_l
 - 4: **if** b_{ij} is from B_l **then**
 - 5: Replace the j th row of A_l with the i th row of $M(:, J_l)$
 - 6: **end if**
 - 7: **if** b_{ij} is from C_l **then**
 - 8: Replace the i th column of A_l with the j th column of $M(I_l, :)$
 - 9: **end if**
 - 10: $l := l + 1$
 - 11: **end while**
-

Algorithm 2 Symmetric Skeleton Decomposition via Maximal Volume

Require: $n \times n$ symmetric matrix M , $r \times r$ submatrix A_0 with $\det(A_0) \neq 0$, tolerance $\epsilon > 0$, $l = 0$, $b_{ij} = \infty$ and $A_l = A_0$

Ensure: A_l a close to dominant submatrix with both row and column indices I_l for M

```
1: while  $|b_{ij}| > 1 + \epsilon$  do
2:   Let  $B_l = M(:, I_l)A_l^{-1}$ , and  $C_l = A_l^{-1}M(I_l, :)$ 
3:   Set  $b_{ij}$  equal to the largest in modulus entry of both  $B_l$  and  $C_l$ 
4:   if  $b_{ij}$  is from  $B_l$  then
5:     Replace the  $j$ th row of  $A_l$  with the  $i$ th row of  $M(:, I_l)$ 
6:     Replace the  $j$ th column of  $A_l$  with the  $i$ th column of  $M(:, I_l)$ 
7:   end if
8:   if  $b_{ij}$  is from  $C_l$  then
9:     Replace the  $i$ th column of  $A_l$  with the  $j$ th column of  $M(I_l, :)$ 
10:    Replace the  $i$ th row of  $A_l$  with the  $j$ th row of  $M(I_l, :)$ 
11:  end if
12:   $l := l + 1$ 
13: end while
```

3 ROM based on optimal transport

Let μ denote the collection of parameters, including time when applicable, and suppose that μ has law Q . We assume that Q is supported on a compact, connected, d -dimensional Riemannian submanifold $\mathcal{M} \subseteq [-b, b]^D$, with $d < D$, and that Q admits a density with respect to the Riemannian volume measure on \mathcal{M} that is bounded above and below by positive constants. For each $\mu \in \mathcal{M}$, let $\rho(\mu)$ denote the probability measure induced by the corresponding parameterized partial differential equation. Let

$$\Omega := [-\xi, \xi]^{D_{\bar{\rho}}},$$

and assume that $\text{supp}(\rho(\mu)) \subseteq \Omega$ for every $\mu \in \mathcal{M}$. Throughout this section, dx denotes the normalized Lebesgue measure on Ω . Finally, we assume that the reference distribution $\bar{\rho} \in \mathcal{P}(\Omega)$ is absolutely continuous with respect to dx ; by a standard abuse of notation, its density is again denoted by $\bar{\rho}$.

Figure 1 and Algorithm 3 summarize the proposed reduced-order modeling framework. Instead of constructing a reduced-order model directly for the solution distributions $\rho(\mu)$, we first map these distributions into a space of transport signatures. For each parameter value μ , we compute the optimal transport potential $\phi(\mu)$ from the reference distribution $\bar{\rho}$ to $\rho(\mu)$, and use this potential to define the transport signature $\Psi(\mu, \cdot)$, as detailed later in this section. This representation is motivated by the observation that, for transport-dominated problems, transport signatures often possess a substantially more favorable low-rank structure than the original distributions, leading to more efficient reduced-order approximations.

Our OT-based ROM procedure consists of three main stages:

1. *Offline stage (i)* (Steps 1 - 3 in Algorithm 3): extracting transport signatures $\Psi(\mu, \cdot)$ from the probability distributions $\rho(\mu)$;

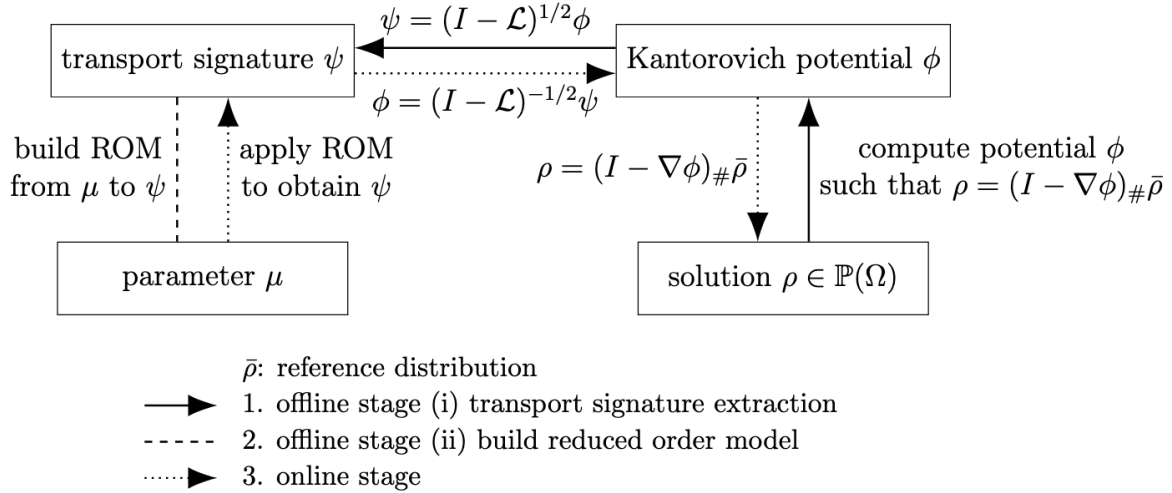


Figure 1: Illustration of the OT-based reduced-order model.

2. *Offline stage (ii)* (Steps 4 - 7 in Algorithm 3): constructing a reduced-order model in the resulting transport-signature space; and
3. *Online stage* (Step 8 in Algorithm 3): predicting the transport signature $\Psi(\mu, \cdot)$ associated with a new parameter value μ , and reconstructing the target probability distribution $\rho(\mu)$ from the predicted signature.

The remainder of this section describes these steps in detail.

Table 1 summarizes key notations in our algorithm and analysis. When sample splitting is not used in computations, the same offline parameter set may be used both for skeleton selection and for training the coefficient map; the split notation is introduced only for the theoretical analysis.

3.1 Offline stage (i): signature extraction

For each $\mu \in \mathcal{M}$, let $\phi(\mu)$ be the Kantorovich potential (see Theorem 1) for the optimal transport from $\bar{\rho}$ to $\rho(\mu)$, normalized by

$$\int_{\Omega} \phi(\mu)(x) dx = 0.$$

Thus, for the quadratic transport cost, the optimal transport map pushing $\bar{\rho}$ forward to $\rho(\mu)$ is

$$T_{\bar{\rho} \rightarrow \rho(\mu)} = I - \nabla \phi(\mu).$$

We collect these Kantorovich potentials and maps into the parameter-dependent functions

$$\Phi : \mathcal{M} \times \Omega \rightarrow \mathbb{R}, \quad \Phi(\mu, \cdot) := \phi(\mu), \quad (16)$$

and

$$\mathbf{T} : \mathcal{M} \times \Omega \rightarrow \mathbb{R}^{D_{\bar{\rho}}}, \quad \mathbf{T}(\mu, \cdot) := T_{\bar{\rho} \rightarrow \rho(\mu)}. \quad (17)$$

By construction,

$$\mathbf{Id}_x - \nabla_x \Phi = \mathbf{T}.$$

We define the weighted Laplacian acting on functions of x by

$$\mathcal{L}f := \nabla_x \cdot (\bar{\rho} \nabla_x f), \quad (18)$$

equipped with a self-adjoint realization on $L^2(\Omega, dx)$ corresponding to boundary conditions for which the integration-by-parts boundary term vanishes. With this sign convention, \mathcal{L} is nonpositive, and hence $I - \mathcal{L}$ is positive and self-adjoint on $L^2(\Omega, dx)$. Therefore, $(I - \mathcal{L})^{1/2}$ is well-defined by the spectral theorem. Moreover,

$$\|(I - \mathcal{L})^{1/2} f\|_{L^2(\Omega, dx)}^2 = \|f\|_{L^2(\Omega, dx)}^2 + \|\nabla_x f\|_{L^2(\Omega, \bar{\rho})}^2 \geq \|\nabla_x f\|_{L^2(\Omega, \bar{\rho})}^2. \quad (19)$$

Equivalently,

$$\|(I - \mathcal{L})^{1/2} f\|_{L^2(\Omega, dx)} \geq \|\nabla_x f\|_{L^2(\Omega, \bar{\rho})}.$$

We define the *transport signature* by

$$\Psi : \mathcal{M} \times \Omega \rightarrow \mathbb{R}, \quad \Psi := (I - \mathcal{L})^{1/2} \Phi. \quad (20)$$

The reduced-order model is then constructed in the transport-signature space, using Ψ rather than Φ . This choice is useful because approximation errors in Ψ directly control the corresponding $L^2(\Omega, \bar{\rho})$ errors in the transport maps $\mathbf{T} = \mathbf{Id}_x - \nabla_x \Phi$.

Remark 1 (Sample splitting in the analysis). Algorithm 3 is written using a single offline data set for simplicity. In the theoretical analysis below, we use a sample-splitting convention: one parameter sample is used to select the skeleton basis, and an independent parameter sample is used to train the coefficient map. This separates the deterministic basis-selection error from the statistical regression error. In computations, the same data set may be reused for both tasks, but the theorem is stated for the split-sample version.

3.2 Offline stage (ii): reduced-order model construction

Throughout this paper, we regard Ψ as a continuous matrix, or cmatrix, whose rows are indexed by $\mu \in \mathcal{M}$ and whose columns are indexed by $x \in \Omega$. Equivalently, Ψ is the kernel of the linear operator

$$H_\Psi : L^2(\Omega, dx) \rightarrow L^2(\mathcal{M}, Q), \quad (H_\Psi f)(\mu) = \int_\Omega \Psi(\mu, x) f(x) dx. \quad (21)$$

For a fixed parameter value $\mu \in \mathcal{M}$, the function $\Psi(\mu, \cdot) \in L^2(\Omega, dx)$ is viewed as a row of the cmatrix. Similarly, for a fixed spatial point $x \in \Omega$, the function $\Psi(\cdot, x) \in L^2(\mathcal{M}, Q)$ is viewed as a column. For index sets $I \subset \mathcal{M}$ and $J \subset \Omega$, the restrictions $\Psi(I, \cdot)$ and $\Psi(\cdot, J)$ play the role of row and column quasi-matrices in the sense of [30]. Hereafter, we will abuse the notation to use I and J to denote both the index sets and the corresponding point subsets in \mathcal{M} and Ω , respectively.

Algorithm 3 ROM via Skeleton Decomposition

Require: PDE solution distributions $\rho(\mu_j)$ with parameters $\{\mu_j\}_{j=1}^n$, reference distribution $\bar{\rho}$, spatial grid $\{x_k\}_{k=1}^m$, unseen parameter μ , and target rank r .

Ensure: Approximation $\hat{\rho}_{n,m}^r(\mu)$ to the solution distribution $\rho(\mu)$.

- 1: Compute the Kantorovich potential $\Phi(\mu_j, \cdot)$ for which the optimal transport map satisfies $T_{\bar{\rho} \rightarrow \rho(\mu_j)} = I - \nabla_x \Phi(\mu_j, \cdot)$, for $j = 1, \dots, n$.
- 2: Let $\Psi(\mu_j, \cdot) := (I - \mathcal{L})^{1/2} \Phi(\mu_j, \cdot)$, for $j = 1, \dots, n$.
- 3: Form the sampled signature matrix $\Psi \in \mathbb{R}^{n \times m}$ with entries $\Psi_{j,k} := \Psi(\mu_j, x_k)$.
- 4: $\Psi \Psi^\top$ $\xrightarrow{\text{symmetric skeleton decomposition (Algorithm 2)}}$ row indices $\{i_s\}_{s=1}^r$, and let $\psi_s(\cdot) := \Psi(\mu_{i_s}, \cdot)$
- 5: For $j = 1, \dots, n$, find the grid-based coefficients $a_m(\mu_j) \in \mathbb{R}^r$ such that

$$\Psi(\mu_j, \cdot) \approx \sum_{s=1}^r a_{m,s}(\mu_j) \psi_s(\cdot)$$

by least-squares fitting on the spatial grid $\{x_k\}_{k=1}^m$.

- 6: Learn the parameter-to-coefficient map $\mu \mapsto a_m(\mu)$ empirically via a feed-forward neural network to obtain the empirical risk minimizer \hat{a}_m .
- 7: Form the rank- r model

$$\hat{\Psi}_{n,m}^r(\mu, x) := \sum_{s=1}^r \hat{a}_{m,s}(\mu) \psi_s(x),$$

and define $\hat{\Phi}_{n,m}^r := (I - \mathcal{L})^{-1/2} \hat{\Psi}_{n,m}^r$ and $\hat{\mathbf{T}}_{n,m}^r(\mu, x) = x - \nabla_x \hat{\Phi}_{n,m}^r(\mu, x)$.

- 8: Obtain the approximation to the density at parameter μ by $\hat{\rho}_{n,m}^r(\mu) := (\hat{\mathbf{T}}_{n,m}^r(\mu, \cdot))_{\#} \bar{\rho}$.
-

Reduced-order basis Let $\nu_1, \dots, \nu_r \in \mathcal{M}$ be selected parameter values. We form a reduced-order basis from the corresponding rows of Ψ by defining

$$\psi : \Omega \rightarrow \mathbb{R}^r, \quad \psi(x) := \begin{pmatrix} \psi_1(x) \\ \vdots \\ \psi_r(x) \end{pmatrix}, \quad \psi_s(\cdot) := \Psi(\nu_s, \cdot), \quad s = 1, \dots, r. \quad (22)$$

For each $\mu \in \mathcal{M}$, we define the best approximation of $\Psi(\mu, \cdot)$ from the selected row span by least-squares projection. Let

$$G := \int_{\Omega} \psi(x) \psi(x)^\top dx \in \mathbb{R}^{r \times r}, \quad b(\mu) := \int_{\Omega} \Psi(\mu, x) \psi(x) dx \in \mathbb{R}^r. \quad (23)$$

Assuming that G is invertible, define

$$a^*(\mu) := G^{-1} b(\mu) = \begin{pmatrix} a_1^*(\mu) \\ \vdots \\ a_r^*(\mu) \end{pmatrix}. \quad (24)$$

The resulting rank- r approximation is

$$\Psi^{*r}(\mu, x) := a^*(\mu)^\top \psi(x) = \sum_{s=1}^r a_s^*(\mu) \psi_s(x). \quad (25)$$

Equivalently, for each fixed $\mu \in \mathcal{M}$, $\Psi^{*r}(\mu, \cdot)$ is the $L^2(\Omega, dx)$ -orthogonal projection of $\Psi(\mu, \cdot)$ onto

$$\text{span}\{\psi_1, \dots, \psi_r\}.$$

In practice, Ψ is observed only at finitely many parameter samples and spatial discretization points. Specifically, suppose that the training parameters $\{\mu_j\}_{j=1}^n$ are drawn independently from Q , and that $\{x_k\}_{k=1}^m$ is a regular or quasi-uniform grid on Ω . These samples define the finite matrix

$$\Psi \in \mathbb{R}^{n \times m}, \quad \Psi_{j,k} := \Psi(\mu_j, x_k), \quad j = 1, \dots, n, \quad k = 1, \dots, m. \quad (26)$$

We select row indices

$$I = \{i_1, \dots, i_r\} \subset \{1, \dots, n\},$$

for example by a max-volume row-selection procedure [1], and set

$$\nu_s := \mu_{i_s}, \quad s = 1, \dots, r.$$

Let $\Psi_I \in \mathbb{R}^{r \times m}$ denote the matrix formed from the selected rows of Ψ , so that

$$(\Psi_I)_{s,k} = \Psi_{i_s,k} = \psi_s(x_k).$$

The grid-based Gram matrix and right-hand side are then

$$G_m := \frac{1}{m} \Psi_I \Psi_I^\top = \frac{1}{m} \sum_{k=1}^m \psi(x_k) \psi(x_k)^\top \in \mathbb{R}^{r \times r}, \quad (27)$$

and

$$b_m(\mu) := \frac{1}{m} \sum_{k=1}^m \Psi(\mu, x_k) \psi(x_k) \in \mathbb{R}^r. \quad (28)$$

Assuming that G_m is invertible, define the grid-based coefficient map

$$a_m : \mathcal{M} \rightarrow \mathbb{R}^r, \quad a_m(\mu) := G_m^{-1} b_m(\mu). \quad (29)$$

This gives the grid-based rank- r approximation

$$\Psi_m^r(\mu, x) := a_m(\mu)^\top \psi(x) = \sum_{s=1}^r a_{m,s}(\mu) \psi_s(x). \quad (30)$$

We also quantify the coverage of the parameter samples and the spatial discretization by the corresponding fill distances h_μ and h_x :

$$h_\mu(n) := \sup_{\mu \in \mathcal{M}} \min_{1 \leq j \leq n} d_{\mathcal{M}}(\mu, \mu_j), \quad h_x(m) := \sup_{x \in \Omega} \min_{1 \leq k \leq m} \|x - x_k\|_2. \quad (31)$$

The discrepancy between the continuous $L^2(\Omega, dx)$ projection Ψ^{*r} and the grid-based projection Ψ_m^r is controlled by the quadrature assumption in Assumption 3 and by the spatial fill distance.

Parameter-to-coefficient map For each sampled parameter μ_j , the coefficient vector $a_m(\mu_j)$ can equivalently be computed by solving the discrete least-squares problem

$$a_m(\mu_j) = \arg \min_{\tilde{a} \in \mathbb{R}^r} \frac{1}{m} \sum_{k=1}^m |\Psi(\mu_j, x_k) - \tilde{a}^\top \psi(x_k)|^2 = \arg \min_{\tilde{a} \in \mathbb{R}^r} \frac{1}{m} \|\Psi_{j,:} - \tilde{a}^\top \Psi_I\|_2^2. \quad (32)$$

We collect these coefficient vectors in the matrix

$$A \in \mathbb{R}^{n \times r}, \quad A_{j,:} = a_m(\mu_j)^\top, \quad j = 1, \dots, n. \quad (33)$$

To evaluate the reduced-order model at a new parameter value, we approximate the parameter-to-coefficient map a_m by a neural network

$$\hat{a} : \mathcal{M} \rightarrow \mathbb{R}^r.$$

Specifically, we seek \hat{a} in the class

$$\mathcal{N}_r(R, \kappa, L, p, K) := \left\{ S : \mathcal{M} \rightarrow \mathbb{R}^r \left| \begin{array}{l} S \text{ is representable by a feedforward neural network} \\ \text{with at most } L \text{ layers and width at most } p, \|S\|_\infty \leq R, \\ \|W_\ell\|_{\infty, \infty} \leq \kappa, \|b_\ell\|_\infty \leq \kappa, \sum_{\ell=1}^L (\|W_\ell\|_0 + \|b_\ell\|_0) \leq K \end{array} \right. \right\}. \quad (34)$$

The neural network is trained by empirical regression against the computed coefficient vectors:

$$\hat{a}_m := \arg \min_{\tilde{a} \in \mathcal{N}_r(R, \kappa, L, p, K)} \frac{1}{n} \sum_{j=1}^n \|\tilde{a}(\mu_j) - a_m(\mu_j)\|_2^2. \quad (35)$$

The final reduced-order approximation of the transport signature is therefore

$$\hat{\Psi}_{n,m}^r(\mu, x) := \hat{a}_m(\mu)^\top \psi(x) = \sum_{s=1}^r \hat{a}_{m,s}(\mu) \psi_s(x). \quad (36)$$

3.3 Online stage

Given the reduced-order approximation $\hat{\Psi}_{n,m}^r$ of the transport signature, we reconstruct an approximation of the target distribution $\rho(\mu)$ by pushing forward the reference distribution $\bar{\rho}$. Specifically, we define

$$\hat{\rho}_{n,m}^r(\mu) := (\hat{\mathbf{T}}_{n,m}^r(\mu, \cdot))_{\#} \bar{\rho}, \quad (37)$$

where

$$\hat{\mathbf{T}}_{n,m}^r(\mu, x) = x - \nabla_x \hat{\Phi}_{n,m}^r(\mu, x), \quad \hat{\Phi}_{n,m}^r := (I - \mathcal{L})^{-1/2} \hat{\Psi}_{n,m}^r. \quad (38)$$

Thus, the reduced-order model for the distribution is obtained by first mapping the predicted transport signature back to a transport potential, then differentiating to obtain the transport map, and finally pushing forward the reference distribution.

Notation	Meaning
<i>Parameterized distributions and reference measure</i>	
μ	Collection of parameters, including time when applicable.
Q	Probability law of μ on the parameter space \mathcal{M} .
\mathcal{M}	Compact, connected, d -dimensional Riemannian submanifold of $[-b, b]^D$.
$\tau_{\mathcal{M}}$	Reach of the manifold \mathcal{M} .
$d_{\mathcal{M}}$	Riemannian distance on \mathcal{M} .
$\rho(\mu)$	Probability measure induced by the parameterized PDE at parameter value μ .
Ω	Spatial domain containing the supports of all solution measures, $\Omega = [-\xi, \xi]^{D_{\bar{\rho}}}$.
dx	Normalized Lebesgue measure on Ω .
$\bar{\rho}$	Reference probability distribution on Ω .
<i>Transport potentials, maps, and signatures</i>	
$\phi(\mu)$	Kantorovich potential for the optimal transport from $\bar{\rho}$ to $\rho(\mu)$; $\int_{\Omega} \phi(\mu)(x) dx = 0$.
$\Phi(\mu, x)$	Parameter-dependent Kantorovich potential, with $\Phi(\mu, \cdot) = \phi(\mu)$.
$\mathbf{T}(\mu, x)$	Optimal transport map from $\bar{\rho}$ to $\rho(\mu)$, given by $\mathbf{T}(\mu, \cdot) = I - \nabla_x \Phi(\mu, \cdot)$.
\mathcal{L}	Weighted Laplacian $\mathcal{L}f = \nabla_x \cdot (\bar{\rho} \nabla_x f)$.
$\Psi(\mu, x)$	Transport-signature kernel, $\Psi = (I - \mathcal{L})^{1/2} \Phi$.
H_{Ψ}	Integral operator with kernel Ψ , $(H_{\Psi}f)(\mu) = \int_{\Omega} \Psi(\mu, x) f(x) dx$.
<i>Samples, grids, and skeleton basis</i>	
n_{skel}	Number of parameter samples used for skeleton selection in the analysis.
$\{\mu_{\ell}^{\text{skel}}\}_{\ell=1}^{n_{\text{skel}}}$	Parameter samples used to select the skeleton basis.
n	Number of parameter samples used to train the coefficient map.
$\{\mu_j^{\text{train}}\}_{j=1}^n$	Independent training samples for learning the map $\mu \mapsto a_m(\mu)$ in the analysis.
m	Number of spatial grid points.
$\{x_k\}_{k=1}^m$	Spatial discretization points in Ω .
r	Target rank of the reduced-order model.
Ψ^{skel}	Sampled signature matrix used for skeleton selection, $\Psi_{\ell, k}^{\text{skel}} = \Psi(\mu_{\ell}^{\text{skel}}, x_k)$.
Ψ	Sampled signature matrix; when no sample splitting is used, $\Psi_{j, k} = \Psi(\mu_j, x_k)$.
I	Selected row indices from the skeleton decomposition, $I = \{i_1, \dots, i_r\}$.
J	Selected column indices from the skeleton decomposition, $J = \{j_1, \dots, j_r\}$.
ν_s	Selected parameter value, $\nu_s = \mu_{i_s}^{\text{skel}}$, for $s = 1, \dots, r$.
ζ_s	Selected spatial point, $\zeta_s = x_{j_s}$, for $s = 1, \dots, r$.
I_{μ}	Selected parameter set, $I_{\mu} = \{\nu_1, \dots, \nu_r\} \subset \mathcal{M}$.
J_x	Selected spatial point set, $J_x = \{\zeta_1, \dots, \zeta_r\} \subset \Omega$.
ψ_s	Selected transport-signature basis function, $\psi_s(\cdot) = \Psi(\nu_s, \cdot)$.
$\psi(x)$	Vector of selected basis functions, $\psi(x) = (\psi_1(x), \dots, \psi_r(x))^{\top}$.
<i>Projection coefficients and reduced approximations</i>	
G	Continuous Gram matrix, $G = \int_{\Omega} \psi(x) \psi(x)^{\top} dx$.
$b(\mu)$	Continuous right-hand side, $b(\mu) = \int_{\Omega} \Psi(\mu, x) \psi(x) dx$.
$a^*(\mu)$	Continuous projection coefficient vector, $a^*(\mu) = G^{-1} b(\mu)$.
Ψ^{*r}	Continuous $L^2(\Omega, dx)$ projection of Ψ onto $\text{span}\{\psi_1, \dots, \psi_r\}$.

G_m	Grid-based Gram matrix, $G_m = \frac{1}{m} \sum_{k=1}^m \psi(x_k) \psi(x_k)^\top$.
$b_m(\mu)$	Grid-based right-hand side, $b_m(\mu) = \frac{1}{m} \sum_{k=1}^m \Psi(\mu, x_k) \psi(x_k)$.
$a_m(\mu)$	Grid-based coefficient vector, $a_m(\mu) = G_m^{-1} b_m(\mu)$.
Ψ_m^r	Grid-based rank- r approximation, $\Psi_m^r(\mu, x) = a_m(\mu)^\top \psi(x)$.
\hat{a}_m	Learned approximation of the grid-based coefficient map a_m .
$\hat{\Psi}_{n,m}^r$	Learned rank- r approximation of Ψ , $\hat{\Psi}_{n,m}^r(\mu, x) = \hat{a}_m(\mu)^\top \psi(x)$.
$\hat{\Phi}_{n,m}^r$	Reconstructed transport potential, $\hat{\Phi}_{n,m}^r = (I - \mathcal{L})^{-1/2} \hat{\Psi}_{n,m}^r$.
$\hat{\mathbf{T}}_{n,m}^r$	Approximated transport map, $\hat{\mathbf{T}}_{n,m}^r(\mu, x) = x - \nabla_x \hat{\Phi}_{n,m}^r(\mu, x)$.
$\hat{\rho}_{n,m}^r(\mu)$	Reconstructed ROM distribution, $\hat{\rho}_{n,m}^r(\mu) = \left(\hat{\mathbf{T}}_{n,m}^r(\mu, \cdot) \right)_{\#} \bar{\rho}$.

Quantities used in the error analysis

$h_\mu^{\text{skel}}(n_{\text{skel}})$	Fill distance of the skeleton-selection parameter sample
$h_x(m)$	Fill distance of the spatial grid, $h_x(m) = \sup_{x \in \Omega} \min_{1 \leq k \leq m} \ x - x_k\ _2$.
Δ_r^{cont}	Maximal continuous $r \times r$ volume of the kernel Ψ .
θ	Fraction of the maximal continuous volume captured by the selected skeleton.
γ_r, Γ_r	Minimum and maximum eigenvalues of the continuous Gram matrix G .
$\sigma_k(\Psi)$	k th singular value of the integral operator H_Ψ .

Table 1: Notation used in the OT-based reduced-order modeling framework.

4 Theoretical Analysis

In this section, we present our main result, Theorem 2, which establishes a mean-squared W_2 error bound between the reconstructed distribution $\hat{\rho}_{n,m}^r(\mu)$ and the true distribution $\rho(\mu)$. We begin by stating a few necessary assumptions.

4.1 Assumptions

We first specify the sample-splitting convention used in the analysis. Let

$$\{\mu_\ell^{\text{skel}}\}_{\ell=1}^{n_{\text{skel}}} \subset \mathcal{M}$$

be the parameter sample used for skeleton selection, and let $\{x_k\}_{k=1}^m \subset \Omega$ be the spatial grid. These samples define the skeleton-selection matrix

$$\Psi^{\text{skel}} \in \mathbb{R}^{n_{\text{skel}} \times m}, \quad \Psi_{\ell,k}^{\text{skel}} := \Psi(\mu_\ell^{\text{skel}}, x_k).$$

A maximum-volume skeleton decomposition selects row indices

$$I = \{i_1, \dots, i_r\} \subset \{1, \dots, n_{\text{skel}}\}$$

and column indices

$$J = \{j_1, \dots, j_r\} \subset \{1, \dots, m\}.$$

We form the reduced basis in (22) by selected parameter and spatial points

$$\nu_s := \mu_{i_s}^{\text{skel}}, \quad \zeta_s := x_{j_s}, \quad s = 1, \dots, r.$$

Conditional on this selected basis and spatial grid, let

$$\{\mu_j^{\text{train}}\}_{j=1}^n$$

be an independent parameter sample drawn from Q . This second sample is used only to train the parameter-to-coefficient map. The continuous projection coefficients are denoted by $a^*(\mu)$, while the grid-based coefficients are denoted by $a_m(\mu)$. Accordingly, Ψ^{*r} denotes the continuous $L^2(\Omega, dx)$ projection, Ψ_m^r denotes its grid-based counterpart, and $\widehat{\Psi}_{n,m}^r$ denotes the learned reduced-order model. The dependence on the skeleton-selection sample is suppressed in the notation, since the statistical estimates are conditional on the selected basis and grid.

We now state the assumptions used to prove the main error bound. The first assumption is geometric and ensures that the parameter space can be treated as a well-behaved compact manifold for sampling and learning estimates.

Assumption 1. We assume that \mathcal{M} has positive reach $\tau_{\mathcal{M}} > 0$, where

$$\tau_{\mathcal{M}} := \sup\{r > 0 : \text{every point within distance } r \text{ of } \mathcal{M} \text{ has a unique nearest point on } \mathcal{M}\}.$$

Our second assumption concerns the regularity of Ψ .

Assumption 2 (Regularity of Ψ). Suppose $\Psi : \mathcal{M} \times \Omega \rightarrow \mathbb{R}$ satisfies the following conditions.

- Ψ is nondegenerate at rank r , in the sense that

$$\Delta_r^{\text{cont}} := \max_{\substack{(\mu_1, \dots, \mu_r) \in \mathcal{M}^r \\ (x_1, \dots, x_r) \in \Omega^r}} \left| \det [\Psi(\mu_i, x_j)]_{i,j=1}^r \right| > 0. \quad (39)$$

- Ψ is Lipschitz continuous with constant $L_{\Psi} > 0$:

$$|\Psi(\mu', x') - \Psi(\mu, x)| \leq L_{\Psi} \sqrt{d_{\mathcal{M}}(\mu, \mu')^2 + \|x' - x\|_2^2},$$

where $d_{\mathcal{M}}$ is the Riemannian distance on \mathcal{M} .

- Ψ is uniformly bounded:

$$\sup_{(\mu, x) \in \mathcal{M} \times \Omega} |\Psi(\mu, x)| \leq U$$

for some constant $U > 0$.

The next assumption concerns the reduced basis and the spatial quadrature rule. It ensures that the selected signatures are linearly independent in $L^2(\Omega, dx)$ and that the grid-based inner products used to compute $a_m(\mu)$ are accurate approximations of the corresponding continuous inner products.

Assumption 3 (Reduced basis and quadrature). Let

$$\psi(x) := (\psi_1(x), \dots, \psi_r(x))^{\top}, \quad G := \int_{\Omega} \psi(x) \psi(x)^{\top} dx, \quad G_m := \frac{1}{m} \sum_{k=1}^m \psi(x_k) \psi(x_k)^{\top}.$$

Assume that:

(i) The Gram matrix G is positive definite, with

$$\gamma_r := \lambda_{\min}(G) > 0, \quad \Gamma_r := \lambda_{\max}(G) < \infty.$$

(ii) The quadrature rule satisfies

$$\left| \int_{\Omega} f(x) dx - \frac{1}{m} \sum_{k=1}^m f(x_k) \right| \leq C_{\text{quad}} \text{Lip}(f) h_x(m)$$

for every Lipschitz function f .

(iii) The fill distance is sufficiently small:

$$h_x(m) \leq \frac{\gamma_r}{4C_{\text{quad}} r U L_{\Psi}},$$

where U and L_{Ψ} are defined in Assumption 2.

The final assumption isolates the low-rank approximation property supplied by the skeleton decomposition. It states that if the selected rows and columns capture a fixed fraction of the maximal continuous volume, then the associated skeleton approximation has an error controlled by the next singular value of the transport-signature kernel.

The column set J_x is used only in the analysis of the skeleton approximation; the reduced-order basis itself is formed from the selected rows $\{\psi_s\}_{s=1}^r$.

Assumption 4 (Low-rank approximation). Consider the kernel function $\Psi : \mathcal{M} \times \Omega \rightarrow \mathbb{R}$. Let

$$I_{\mu} = \{\nu_1, \dots, \nu_r\} \subset \mathcal{M}, \quad J_x = \{\zeta_1, \dots, \zeta_r\} \subset \Omega$$

be selected parameter and spatial point sets. Suppose that

$$|\det \Psi(I_{\mu}, J_x)| \geq \theta \Delta_r^{\text{cont}}, \quad \text{for some } \theta \in (0, 1],$$

where Δ_r^{cont} is defined in (39). Define the continuous skeleton approximation

$$\Psi_r^{\text{skel}}(\mu, x) := \Psi(\mu, J_x) [\Psi(I_{\mu}, J_x)]^{-1} \Psi(I_{\mu}, x). \quad (40)$$

Assume that

$$\|\Psi - \Psi_r^{\text{skel}}\|_{L^{\infty}(\mathcal{M} \times \Omega)} \leq \frac{C(r+1)}{\theta} \sigma_{r+1}(\Psi),$$

where $\sigma_{r+1}(\Psi)$ denotes the $(r+1)$ -th singular value of the operator H_{Ψ} in (21). The constant C is independent of θ , r , and the particular kernel Ψ , but may depend on the regularity class under consideration.

Remark 2 (Motivation for Assumption 4). Assumption 4 is the continuous-kernel analogue of the classical max-volume skeleton approximation bound for finite matrices. Indeed, it was established in [1] that, if $A \in \mathbb{R}^{m \times n}$ and $A_{I,J}$ has volume at least a fraction $\theta \in (0, 1]$ of the maximum $r \times r$ volume, then the skeleton approximation

$$A_{:,J} A_{I,J}^{-1} A_{I,:}$$

satisfies a Chebyshev-norm estimate of the form

$$\|A - A_{:,J}A_{I,J}^{-1}A_{I,:}\|_C \leq \frac{r+1}{\theta \sqrt{\sum_{k=1}^{r+1} \sigma_k^{-2}(A)}} \leq \frac{r+1}{\theta} \sigma_{r+1}(A).$$

Assumption 4 postulates the corresponding bound for the continuous matrix $\Psi(\mu, x)$, with the matrix maximum norm replaced by $L^\infty(\mathcal{M} \times \Omega)$ and the matrix singular values replaced by the singular values of the integral operator H_Ψ in (21).

4.2 Main Result

Before stating the main theorem, we record two auxiliary facts. The first transfers error estimates for transport maps into W_2 error estimates for the corresponding pushforward measures. The second relates the maximal volume of a sampled matrix to the maximal volume of the underlying continuous kernel; this justifies using a discrete skeleton decomposition to select representative transport signatures.

Lemma 1. *Let λ be a probability measure on a compact domain $\Omega \subseteq \mathbb{R}^{D_{\bar{p}}}$. Let $\rho_1 := (T_1)_\# \lambda$ and $\rho_2 := (T_2)_\# \lambda$, where $T_1, T_2 \in L^2(\lambda)$. Then*

$$W_2^2(\rho_1, \rho_2) \leq \|T_1 - T_2\|_{L^2(\lambda)}^2. \quad (41)$$

Proof. Let us define a coupling map π between ρ_1 and ρ_2 by pushing λ forward through the map (T_1, T_2) , i.e., $\pi := (T_1, T_2)_\# \lambda$. Then π has the first marginal $(T_1)_\# \lambda = \rho_1$ and second marginal $(T_2)_\# \lambda = \rho_2$, so $\pi \in \Pi(\rho_1, \rho_2)$. By the definition of 2-Wasserstein distance,

$$W_2^2(\rho_1, \rho_2) = \inf_{\gamma \in \Pi(\rho_1, \rho_2)} \int |y - z|^2 d\gamma(y, z) \leq \int |y - z|^2 d\pi(y, z).$$

Now compute the cost under π using the pushforward definition,

$$\int |y - z|^2 d\pi(y, z) = \int_{\Omega} |T_1(x) - T_2(x)|^2 d\lambda(x) = \|T_1 - T_2\|_{L^2(\lambda)}^2.$$

Combining the two inequalities gives the desired result. \square

Lemma 2. *Let Assumption 2 hold and set $\Omega = [-\xi, \xi]^{D_{\bar{p}}}$. Let $\{\mu_j\}_{j=1}^n \subset \mathcal{M}$ and $\{x_k\}_{k=1}^m \subset \Omega$ be sampling sets and define the sampled matrix $\Psi \in \mathbb{R}^{n \times m}$ by (26). Define $\varepsilon_{n,m} := L_\Psi(h_\mu(n) + h_x(m))$.*

For $r \geq 1$, define the continuous and discrete maximal volumes

$$\Delta_r^{\text{cont}} := \sup_{\substack{I_\mu \subset \mathcal{M}, J_x \subset \Omega \\ |I_\mu| = |J_x| = r}} |\det \Psi(I_\mu, J_x)|, \quad \Delta_r^{\text{disc}} := \max_{\substack{I \subset \{1, \dots, n\}, J \subset \{1, \dots, m\} \\ |I| = |J| = r}} |\det \Psi(I, J)|.$$

Let $C_r := r^{\frac{r}{2}+1}$. Then

$$\Delta_r^{\text{disc}} \geq \Delta_r^{\text{cont}} - C_r U^{r-1} \varepsilon_{n,m}.$$

Consequently, defining

$$\theta_{n,m} := \max \left\{ 0, 1 - \frac{C_r U^{r-1} L_{\Psi}(h_{\mu}(n) + h_x(m))}{\Delta_r^{\text{cont}}} \right\} \in [0, 1],$$

we obtain

$$\Delta_r^{\text{disc}} \geq \theta_{n,m} \Delta_r^{\text{cont}}.$$

In particular, if

$$h_{\mu}(n) + h_x(m) < \frac{\Delta_r^{\text{cont}}}{C_r U^{r-1} L_{\Psi}},$$

then $\theta_{n,m} \in (0, 1]$.

Proof. By Assumption 2, Ψ is Lipschitz and therefore continuous on the compact set $\mathcal{M} \times \Omega$. Hence the map

$$(\mu_1, \dots, \mu_r, x_1, \dots, x_r) \mapsto \det(\Psi(\mu_i, x_j))_{i,j=1}^r$$

is continuous on the compact set $(\mathcal{M}^r) \times (\Omega^r)$, and therefore the supremum defining Δ_r^{cont} is attained. Thus there exist $I^* = \{\mu_1^*, \dots, \mu_r^*\} \subset \mathcal{M}$ and $J^* = \{x_1^*, \dots, x_r^*\} \subset \Omega$ such that

$$\Delta_r^{\text{cont}} = |\det A|, \quad A := (\Psi(\mu_i^*, x_j^*))_{i,j=1}^r.$$

For sufficiently small fill distances, these sampled representatives may be chosen to be distinct, since the maximizing tuples have nonzero determinant and hence consist of distinct parameter and spatial points.

By definition of the fill distances $h_{\mu}(n)$ and $h_x(m)$, for each μ_i^* there exists $\widehat{i}_i \in \{1, \dots, n\}$ such that

$$d_{\mathcal{M}}(\mu_i^*, \mu_{\widehat{i}_i}) \leq h_{\mu}(n),$$

and for each x_j^* there exists $\widehat{j}_j \in \{1, \dots, m\}$ such that

$$\|x_j^* - x_{\widehat{j}_j}\|_2 \leq h_x(m).$$

Let $\widehat{I} = \{\widehat{i}_1, \dots, \widehat{i}_r\}$ and $\widehat{J} = \{\widehat{j}_1, \dots, \widehat{j}_r\}$, and define

$$\widehat{A} := \Psi(\widehat{I}, \widehat{J}) = (\Psi(\mu_{\widehat{i}_i}, x_{\widehat{j}_j}))_{i,j=1}^r.$$

By the Lipschitz continuity of Ψ ,

$$|\widehat{A}_{ij} - A_{ij}| = |\Psi(\mu_{\widehat{i}_i}, x_{\widehat{j}_j}) - \Psi(\mu_i^*, x_j^*)| \leq L_{\Psi}(h_{\mu}(n) + h_x(m)) = \varepsilon_{n,m}.$$

Hence $\widehat{A} = A + E$ with $|E_{ij}| \leq \varepsilon_{n,m}$.

Let a_1, \dots, a_r denote the columns of A and e_1, \dots, e_r the columns of E . Using a telescoping expansion in the columns and Hadamard's inequality,

$$|\det(A + E) - \det(A)| \leq \sum_{\ell=1}^r |\det(\widehat{a}_1, \dots, \widehat{a}_{\ell-1}, e_{\ell}, a_{\ell+1}, \dots, a_r)|,$$

where a_ℓ and \widehat{a}_ℓ are the ℓ th columns of A and $\widehat{A} = A + E$, respectively, and $e_\ell = \widehat{a}_\ell - a_\ell$. Since both A and \widehat{A} have entries bounded by U , their columns have Euclidean norm at most $\sqrt{r}U$, while $\|e_\ell\|_2 \leq \sqrt{r}\varepsilon_{n,m}$. Hence

$$|\det(A + E) - \det(A)| \leq r(\sqrt{r}\varepsilon_{n,m})(\sqrt{r}U)^{r-1} = C_r U^{r-1} \varepsilon_{n,m}, \quad C_r = r^{\frac{r}{2}+1}.$$

Consequently,

$$|\det \widehat{A}| \geq |\det A| - |\det(\widehat{A}) - \det(A)| \geq \Delta_r^{\text{cont}} - C_r U^{r-1} \varepsilon_{n,m}.$$

Since Δ_r^{disc} is the maximal determinant over all sampled $r \times r$ submatrices, it follows that

$$\Delta_r^{\text{disc}} \geq |\det \Psi(\widehat{I}, \widehat{J})| = |\det \widehat{A}| \geq \Delta_r^{\text{cont}} - C_r U^{r-1} \varepsilon_{n,m}.$$

Dividing by Δ_r^{cont} and defining

$$\theta_{n,m} = \max \left\{ 0, 1 - \frac{C_r U^{r-1} L_\Psi (h_\mu(n) + h_x(m))}{\Delta_r^{\text{cont}}} \right\},$$

yields

$$\Delta_r^{\text{disc}} \geq \theta_{n,m} \Delta_r^{\text{cont}}.$$

□

We now state the main result, which establishes a mean-squared W_2 generalization error bound between the reconstructed distribution $\widehat{\rho}_{n,m}^r(\mu)$ and the true distribution $\rho(\mu)$.

Theorem 2. *Suppose Assumptions 1–4 hold under the sample-splitting convention described above. Let*

$$I_\mu = \{\nu_1, \dots, \nu_r\} \subset \mathcal{M}, \quad J_x = \{\zeta_1, \dots, \zeta_r\} \subset \Omega$$

be the selected parameter and spatial point sets, and suppose that

$$|\det \Psi(I_\mu, J_x)| \geq \theta \Delta_r^{\text{cont}} \tag{42}$$

for some $\theta \in (0, 1]$. Conditional on this selected basis and grid, let \widehat{a}_m be the empirical risk minimizer in (35) over the network class $\mathcal{N}_r(R, \kappa, L, p, K)$ defined in (34). Choose $R \geq R_a$ where $R_a := \frac{2\sqrt{r}U^2}{\gamma_r}$, and choose the remaining network parameters as

$$L = \tilde{O} \left(\frac{\log n}{2+d} \right), \quad p = \tilde{O} \left(r n^{\frac{d}{2+d}} \right), \quad K = \tilde{O} \left(\frac{r}{2+d} n^{\frac{d}{2+d}} \log n \right), \quad \kappa = O(\max\{1, b, \sqrt{d}, \tau_{\mathcal{M}}^2\}).$$

Let $\sigma_k(\Psi)$ denote the k th singular value of the integral operator H_Ψ in (21). Then

$$\begin{aligned} & \mathbb{E} \left[\int_{\mathcal{M}} W_2^2(\rho(\mu), \widehat{\rho}_{n,m}^r(\mu)) dQ(\mu) \right] \\ & \leq \frac{4C^2(r+1)^2 \sigma_{r+1}^2(\Psi)}{\theta^2} + 4C_1 \Gamma_r h_x(m)^2 + 2c\Gamma_r \frac{r^2 U^4}{\gamma_r^2} \left(n^{-\frac{2}{2+d}} + \frac{D}{n} \right) \log^3 n. \end{aligned} \tag{43}$$

Here C_1 is the constant that depends only on $r, \gamma_r, U, L_\Psi, C_{\text{quad}}$, and c is a constant depending on $\log D, d, b, \kappa, \mathcal{M}$, and the Lipschitz radius of the coefficient functions. The notation $\tilde{O}(\cdot)$ hides factors depending on d and some logarithmic factors.

Moreover, if the skeleton-selection parameter sample and spatial grid have fill distances

$$h_\mu^{\text{skel}}(n_{\text{skel}}) := \sup_{\mu \in \mathcal{M}} \min_{1 \leq \ell \leq n_{\text{skel}}} d_{\mathcal{M}}(\mu, \mu_\ell^{\text{skel}})$$

and $h_x(m)$, then the volume condition (42) holds with

$$\theta = 1 - \frac{C_{\text{det}}(r)U^{r-1}L_\Psi(h_\mu^{\text{skel}}(n_{\text{skel}}) + h_x(m))}{\Delta_r^{\text{cont}}},$$

provided the right-hand side is positive.

The proof decomposes the total error into three terms. The first is the deterministic low-rank approximation error from representing Ψ by the span of the selected signatures. The second is the discretization error from replacing continuous $L^2(\Omega, dx)$ projections by grid-based least-squares projections. The third is the statistical error from learning the parameter-to-coefficient map a_m from finitely many training samples. We estimate these three contributions separately and then combine them in the proof of Theorem 2.

• **Low-rank approximation error.** We first control the error from approximating the transport-signature kernel Ψ by the span of the selected signatures $\{\psi_s\}_{s=1}^r$. Assumption 4 gives a skeleton approximation bound in $L^\infty(\mathcal{M} \times \Omega)$; the following lemma transfers this bound to the continuous $L^2(\Omega, dx)$ projection Ψ^{*r} used in the ROM construction.

Lemma 3 (Low-rank error). *Let Ψ^{*r} be the continuous $L^2(\Omega, dx)$ projection defined in (25). Suppose Assumptions 1–4 hold. Then*

$$\|\Psi - \Psi^{*r}\|_{L^2(Q; L^2(dx))} \leq \frac{C(r+1)}{\theta} \sigma_{r+1}(\Psi), \quad (44)$$

where C is the constant from Assumption 4.

Proof. By definition, for each fixed μ , $\Psi^{*r}(\mu, \cdot)$ is the $L^2(\Omega, dx)$ -orthogonal projection of $\Psi(\mu, \cdot)$ onto $\text{span}\{\psi_1, \dots, \psi_r\}$. Therefore, for any admissible coefficient map $\tilde{a} : \mathcal{M} \rightarrow \mathbb{R}^r$,

$$\|\Psi - \Psi^{*r}\|_{L^2(Q; L^2(dx))} \leq \|\Psi - \tilde{a}(\cdot)^\top \psi(\cdot)\|_{L^2(Q; L^2(dx))}.$$

Taking

$$\tilde{a}(\mu)^\top = \Psi(\mu, J_x) [\Psi(I_\mu, J_x)]^{-1}$$

gives

$$\|\Psi - \Psi^{*r}\|_{L^2(Q; L^2(dx))} \leq \|\Psi - \Psi_r^{\text{skel}}\|_{L^2(Q; L^2(dx))}.$$

Since Q and dx are probability measures,

$$\|\Psi - \Psi_r^{\text{skel}}\|_{L^2(Q; L^2(dx))} \leq \|\Psi - \Psi_r^{\text{skel}}\|_{L^\infty(\mathcal{M} \times \Omega)}.$$

The result now follows from Assumption 4. □

• **Discretization error.** We next compare the ideal continuous projection Ψ^{*r} with the grid-based projection Ψ_m^r used by the algorithm. This is the only place where the spatial quadrature error enters the deterministic part of the analysis.

Lemma 4 (Discretization error). *Suppose Assumptions 1–3 hold. Then*

$$\|\Psi^{*r} - \Psi_m^r\|_{L^2(Q;L^2(dx))}^2 \leq C_1 \Gamma_r h_x(m)^2, \quad (45)$$

where C_1 depends only on $r, \gamma_r, U, L_\Psi, C_{\text{quad}}$.

Proof. Notice that

$$\Psi^{*r}(\mu, \cdot) - \Psi_m^r(\mu, \cdot) = \sum_{s=1}^r (a_s^*(\mu) - a_{m,s}(\mu)) \psi_s(\cdot).$$

Therefore,

$$\|\Psi^{*r} - \Psi_m^r\|_{L^2(Q;L^2(dx))}^2 = \int_{\mathcal{M}} (a^*(\mu) - a_m(\mu))^\top G (a^*(\mu) - a_m(\mu)) dQ(\mu) \leq \Gamma_r \|a^* - a_m\|_{L^2(Q;\mathbb{R}^r)}^2.$$

Thus it remains to estimate $\|a^* - a_m\|_{L^2(Q;\mathbb{R}^r)}$.

We first control $G_m - G$. For each $i, j \in \{1, \dots, r\}$, the function $x \mapsto \psi_i(x)\psi_j(x)$ is Lipschitz and satisfies

$$\text{Lip}(\psi_i\psi_j) \leq \|\psi_i\|_{L^\infty} \text{Lip}(\psi_j) + \|\psi_j\|_{L^\infty} \text{Lip}(\psi_i) \leq 2UL_\Psi.$$

Hence, by Assumption 3 (ii),

$$|(G_m - G)_{ij}| \leq 2C_{\text{quad}}UL_\Psi h_x(m).$$

Therefore,

$$\|G_m - G\|_2 \leq r \max_{i,j} |(G_m - G)_{ij}| \leq 2C_{\text{quad}}rUL_\Psi h_x(m).$$

Since Assumption 3 (iii) gives

$$h_x(m) \leq \frac{\gamma_r}{4C_{\text{quad}}rUL_\Psi},$$

we have

$$\|G_m - G\|_2 \leq \frac{\gamma_r}{2}.$$

By Weyl's inequality,

$$\lambda_{\min}(G_m) \geq \frac{\gamma_r}{2}, \quad \|G_m^{-1}\|_2 \leq \frac{2}{\gamma_r}.$$

Next we control $b_m - b$. For each $i \in \{1, \dots, r\}$ and fixed $\mu \in \mathcal{M}$, the function

$$x \mapsto \Psi(\mu, x)\psi_i(x)$$

is Lipschitz with constant at most $2UL_\Psi$. Hence

$$|(b_m(\mu) - b(\mu))_i| \leq 2C_{\text{quad}}UL_\Psi h_x(m),$$

and therefore

$$\|b_m - b\|_{L^2(Q; \mathbb{R}^r)} \leq 2\sqrt{r} C_{\text{quad}} U L_{\Psi} h_x(m).$$

By definition,

$$a^*(\mu) = G^{-1}b(\mu), \quad a_m(\mu) = G_m^{-1}b_m(\mu).$$

Thus, for Q -a.e. μ ,

$$a^*(\mu) - a_m(\mu) = G_m^{-1}(b(\mu) - b_m(\mu)) + G_m^{-1}(G_m - G)a^*(\mu).$$

Taking $L^2(Q; \mathbb{R}^r)$ norms gives

$$\|a^* - a_m\|_{L^2(Q; \mathbb{R}^r)} \leq \|G_m^{-1}\|_2 \left(\|b - b_m\|_{L^2(Q; \mathbb{R}^r)} + \|G_m - G\|_2 \|a^*\|_{L^2(Q; \mathbb{R}^r)} \right).$$

Moreover, since

$$\|b(\mu)\|_2 \leq \sqrt{r} U^2,$$

we have

$$\|a^*(\mu)\|_2 \leq \frac{\sqrt{r} U^2}{\gamma_r} =: R_*.$$

Combining the previous bounds yields

$$\|a^* - a_m\|_{L^2(Q; \mathbb{R}^r)} \leq \frac{4C_{\text{quad}} U L_{\Psi} \sqrt{r}}{\gamma_r} (1 + rR_*) h_x(m),$$

which finishes the proof. \square

• **Statistical error.** Finally, we estimate the error caused by learning the coefficient map $a_m : \mathcal{M} \rightarrow \mathbb{R}^r$ from finitely many parameter samples. For this part of the analysis, it is convenient to use a sample-splitting convention: the skeleton basis is first selected and then held fixed, and an independent training sample is used to learn a_m .

We work under the sample-splitting convention introduced at the beginning of this section. Thus the selected basis and spatial grid are fixed, and the only randomness in the following estimate comes from the independent training sample $\{\mu_j^{\text{train}}\}_{j=1}^n$ used to learn a_m .

The mean-squared statistical error satisfies the following lemma, whose proof uses [8, Theorem 2].

Lemma 5 (Statistical error). *Suppose Assumptions 1–3 hold. Conditional on the selected basis and spatial grid, let $\{\mu_j^{\text{train}}\}_{j=1}^n$ be i.i.d. samples from Q . Let \hat{a}_m be the empirical risk minimizer in (35) over the feedforward neural network class $\mathcal{N}_r(R, \kappa, L, p, K)$ defined in (34), with parameters chosen as*

$$L = \tilde{O} \left(\frac{1}{2+d} \log n \right), \quad p = \tilde{O} \left(r n^{\frac{d}{2+d}} \right), \quad K = \tilde{O} \left(\frac{r}{2+d} n^{\frac{d}{2+d}} \log n \right),$$

$$R \geq \frac{2\sqrt{r} U^2}{\gamma_r}, \quad \kappa = O(\max\{1, b, \sqrt{d}, \tau_{\mathcal{M}}^2\}).$$

Then

$$\mathbb{E} \left[\|\Psi_m^r - \widehat{\Psi}_{n,m}^r\|_{L^2(Q;L^2(dx))}^2 \right] \leq c\Gamma_r \frac{r^2 U^4}{\gamma_r^2} \left(n^{-\frac{2}{2+d}} + \frac{D}{n} \right) \log^3 n, \quad (46)$$

where the expectation is taken over the training samples and c is a constant depending on $\log D$, d , b , κ , \mathcal{M} , and the coefficient Lipschitz radius.

Proof of Lemma 5. Since

$$\Psi_m^r(\mu, \cdot) = \sum_{s=1}^r a_{m,s}(\mu) \psi_s(\cdot), \quad \widehat{\Psi}_{n,m}^r(\mu, \cdot) = \sum_{s=1}^r \widehat{a}_{m,s}(\mu) \psi_s(\cdot),$$

we have

$$\Psi_m^r(\mu, \cdot) - \widehat{\Psi}_{n,m}^r(\mu, \cdot) = \sum_{s=1}^r (a_{m,s}(\mu) - \widehat{a}_{m,s}(\mu)) \psi_s(\cdot).$$

Let

$$e_a(\mu) := (a_{m,1}(\mu) - \widehat{a}_{m,1}(\mu), \dots, a_{m,r}(\mu) - \widehat{a}_{m,r}(\mu))^\top.$$

Then, for each fixed μ ,

$$\left\| \sum_{s=1}^r (a_{m,s}(\mu) - \widehat{a}_{m,s}(\mu)) \psi_s(\cdot) \right\|_{L^2(dx)}^2 = e_a(\mu)^\top G e_a(\mu) \leq \Gamma_r \|e_a(\mu)\|_2^2.$$

Hence

$$\mathbb{E} \left[\|\Psi_m^r - \widehat{\Psi}_{n,m}^r\|_{L^2(Q;L^2(dx))}^2 \right] \leq \Gamma_r \sum_{s=1}^r \mathbb{E} \left[\int_{\mathcal{M}} (a_{m,s}(\mu) - \widehat{a}_{m,s}(\mu))^2 dQ(\mu) \right].$$

We next verify that the target coefficient functions $a_{m,s}$ satisfy the boundedness and Lipschitz conditions required by the neural-network theorem. Since

$$a_m(\mu) = G_m^{-1} b_m(\mu),$$

we have

$$\|a_m(\mu)\|_2 \leq \|G_m^{-1}\|_2 \|b_m(\mu)\|_2.$$

For each s ,

$$|(b_m(\mu))_s| = \left| \frac{1}{m} \sum_{k=1}^m \Psi(\mu, x_k) \psi_s(x_k) \right| \leq U^2.$$

Thus

$$\|b_m(\mu)\|_2 \leq \sqrt{r} U^2.$$

Using $\|G_m^{-1}\|_2 \leq 2/\gamma_r$, we obtain

$$\|a_m(\mu)\|_2 \leq \frac{2\sqrt{r} U^2}{\gamma_r}.$$

In particular,

$$\|a_{m,s}\|_{L^\infty(\mathcal{M})} \leq \frac{2\sqrt{r}U^2}{\gamma_r}, \quad s = 1, \dots, r.$$

Similarly, for $\mu, \mu' \in \mathcal{M}$,

$$|(b_m(\mu) - b_m(\mu'))_s| \leq \frac{1}{m} \sum_{k=1}^m |\Psi(\mu, x_k) - \Psi(\mu', x_k)| |\psi_s(x_k)| \leq UL_{\Psi} d_{\mathcal{M}}(\mu, \mu').$$

Therefore,

$$\|b_m(\mu) - b_m(\mu')\|_2 \leq \sqrt{r} UL_{\Psi} d_{\mathcal{M}}(\mu, \mu'),$$

and hence

$$\|a_m(\mu) - a_m(\mu')\|_2 \leq \frac{2\sqrt{r}UL_{\Psi}}{\gamma_r} d_{\mathcal{M}}(\mu, \mu').$$

Thus each coordinate $a_{m,s}$ is Lipschitz with constant at most $\frac{2\sqrt{r}UL_{\Psi}}{\gamma_r}$.

Applying [8, Theorem 2] to each coefficient function $a_{m,s}$, we obtain

$$\mathbb{E} \left[\int_{\mathcal{M}} (a_{m,s}(\mu) - \widehat{a}_{m,s}(\mu))^2 dQ(\mu) \right] \leq c \left(\frac{2\sqrt{r}U^2}{\gamma_r} \right)^2 \left(n^{-\frac{2}{2+d}} + \frac{D}{n} \right) \log^3 n.$$

Summing over $s = 1, \dots, r$ gives

$$\mathbb{E} \left[\|\Psi_m^r - \widehat{\Psi}_{n,m}^r\|_{L^2(Q; L^2(dx))}^2 \right] \leq c\Gamma_r \frac{r^2 U^4}{\gamma_r^2} \left(n^{-\frac{2}{2+d}} + \frac{D}{n} \right) \log^3 n.$$

The right-hand side has no explicit m -dependence because the bound $\|G_m^{-1}\|_2 \leq 2/\gamma_r$ is uniform once Assumption 3(iii) holds. The m -dependence is isolated in the discretization error. \square

• **Combining the errors together.** We now combine the three estimates. The transport-map error is first converted to a W_2 error using Lemma 1. The definition of the transport signature then converts the transport-map error into an $L^2(Q; L^2(dx))$ error for Ψ . Finally, the latter is decomposed into the low-rank, discretization, and statistical terms estimated above.

Proof of Theorem 2. The 2-Wasserstein distance in (43) can be bounded by the $\bar{\rho}$ -weighted L^2 error between the corresponding transport maps as a result of Lemma 1. Indeed, the coupling $(\mathbf{T}(\mu, \cdot), \widehat{\mathbf{T}}_{n,m}^r(\mu, \cdot))_{\# \bar{\rho}}$ gives

$$W_2^2(\rho(\mu), \widehat{\rho}_{n,m}^r(\mu)) \leq \|\mathbf{T}(\mu, \cdot) - \widehat{\mathbf{T}}_{n,m}^r(\mu, \cdot)\|_{L^2(\bar{\rho})}^2.$$

Define

$$\Phi_m^r := (I - \mathcal{L})^{-1/2} \Psi_m^r, \quad \widehat{\Phi}_{n,m}^r := (I - \mathcal{L})^{-1/2} \widehat{\Psi}_{n,m}^r.$$

Then

$$\begin{aligned}
& \mathbb{E} \left[\int_{\mathcal{M}} W_2^2(\rho(\mu), \widehat{\rho}_{n,m}^r(\mu)) dQ(\mu) \right] \\
& \leq \mathbb{E} \left[\int_{\mathcal{M}} \|\nabla_x \Phi(\mu, \cdot) - \nabla_x \widehat{\Phi}_{n,m}^r(\mu, \cdot)\|_{L^2(\bar{\rho})}^2 dQ(\mu) \right] \\
& \leq 2 \int_{\mathcal{M}} \|\nabla_x \Phi(\mu, \cdot) - \nabla_x \Phi_m^r(\mu, \cdot)\|_{L^2(\bar{\rho})}^2 dQ(\mu) + 2\mathbb{E} \left[\int_{\mathcal{M}} \|\nabla_x \Phi_m^r(\mu, \cdot) - \nabla_x \widehat{\Phi}_{n,m}^r(\mu, \cdot)\|_{L^2(\bar{\rho})}^2 dQ(\mu) \right] \\
& \leq 2 \int_{\mathcal{M}} \|\Psi(\mu, \cdot) - \Psi_m^r(\mu, \cdot)\|_{L^2(dx)}^2 dQ(\mu) + 2\mathbb{E} \left[\int_{\mathcal{M}} \|\Psi_m^r(\mu, \cdot) - \widehat{\Psi}_{n,m}^r(\mu, \cdot)\|_{L^2(dx)}^2 dQ(\mu) \right] \\
& = 2\|\Psi - \Psi_m^r\|_{L^2(Q;L^2(dx))}^2 + 2\mathbb{E} \left[\|\Psi_m^r - \widehat{\Psi}_{n,m}^r\|_{L^2(Q;L^2(dx))}^2 \right] \\
& \leq 4 \underbrace{\|\Psi - \Psi^{*r}\|_{L^2(Q;L^2(dx))}^2}_{\text{low-rank error}} + 4 \underbrace{\|\Psi^{*r} - \Psi_m^r\|_{L^2(Q;L^2(dx))}^2}_{\text{discretization error}} + 2 \underbrace{\mathbb{E} \left[\|\Psi_m^r - \widehat{\Psi}_{n,m}^r\|_{L^2(Q;L^2(dx))}^2 \right]}_{\text{statistical error}} \quad (47) \\
& \leq \frac{4C^2(r+1)^2\sigma_{r+1}^2(\Psi)}{\theta^2} + 4C_1 \Gamma_r h_x(m)^2 + 2c\Gamma_r \frac{r^2 U^4}{\gamma_r^2} \left(n^{-\frac{2}{2+d}} + \frac{D}{n} \right) \log^3 n,
\end{aligned}$$

as desired. The first inequality follows from the coupling induced by the two maps from the reference measure $\bar{\rho}$; see Lemma 1. The second and fourth inequalities follow from $\|A - C\|^2 \leq 2\|A - B\|^2 + 2\|B - C\|^2$. The third inequality uses the identity (19). Moreover, the last part of the statement in Theorem 2 follows directly from Lemma 2. This completes the proof. \square

5 Numerical results

We demonstrate the proposed method on a two-dimensional continuity equation. All numerical experiments are implemented in Python on a PC with an Apple M5 Pro chip and 24 GB of memory¹.

Consider the continuity equation on $[0, 1]^2$ with periodic boundary conditions

$$\begin{cases} \partial_t \rho + \nabla \cdot (\rho v) = 0, & (x, t) \in [0, 1]^2 \times (0, 1], \\ \rho(x, 0) = \rho_0(x), & x \in [0, 1]^2. \end{cases} \quad (48)$$

Here, ρ_0 is an isotropic Gaussian with mean $(0.5, 0.5)$ and standard deviation 0.1. Let the parameter be $\mu = (\alpha, \beta, t)$ and $v(x) = (\alpha \cos(2\pi x_2), \beta \sin(2\pi x_1))$. Then $\rho(\mu)$ denotes the solution to (48) at time t with the velocity field determined by α and β .

5.1 Implementation

For integers n_x, n_t , define $\Delta x = 1/n_x$, $\Delta t = 1/n_t$, spatial points $x_k = ((k_1 - \frac{1}{2})\Delta x, (k_2 - \frac{1}{2})\Delta x)$ for $k = (k_1, k_2)$, and time points $t_l = l\Delta t$. Use $e_1 = (1, 0)$ and $e_2 = (0, 1)$ for index shifts. For

¹The code to reproduce the numerical results in this paper is available at https://github.com/jiajia-yu/rom_transport.

a space-time function u , its grid representation is also denoted by u , with $u_k^l \approx u(x_k, t_l)$. For a probability density ρ , we normalize its grid representation so that $(\Delta x)^2 \sum_{k_1, k_2=1}^{n_x} \rho_k = 1$.

The full-order model (FOM) uses a semi-implicit Lax–Friedrichs scheme with periodic boundary conditions. For a function u defined on the grid, the elementary discrete differential operators are

$$(D_i u)_k = \frac{u_{k+e_i} - u_{k-e_i}}{2\Delta x}, \quad (\Delta_i u)_k = \frac{u_{k+e_i} - 2u_k + u_{k-e_i}}{(\Delta x)^2}, \quad i = 1, 2.$$

Periodic indexing is imposed by $u_{(0, k_2)} = u_{(n_x, k_2)}$, $u_{(k_1, 0)} = u_{(k_1, n_x)}$, and $u_{(n_x+1, k_2)} = u_{(1, k_2)}$, $u_{(k_1, n_x+1)} = u_{(k_1, 1)}$. For the initial density ρ^0 and time-independent velocity $v = (v_1, v_2)$ defined on the grid, the update reads

$$\frac{\rho_k^{l+1} - \rho_k^l}{\Delta t} - \nu_{\text{num}} \Delta x (\Delta_1 \rho^{l+1} + \Delta_2 \rho^{l+1})_k + (D_1(\rho^{l+1} v_1^l) + D_2(\rho^{l+1} v_2^l))_k = 0. \quad (49)$$

We sample 10 independent pairs of (α, β) from $U[-0.4, 0.4]$. For each pair, we solve the equation with the full-order model on a grid with $n_x = n_t = 100$. This yields 1000 samples of $(\mu, \rho(\mu))$ where $\mu = (\alpha, \beta, t)$ and each $\rho(\mu)$ is defined on $m = n_x^2$ grid points. We then sample $n = 200$ of these pairs as μ_j and $\rho(\mu_j)$, $j = 1, \dots, n$, to learn the reduced order model.

Offline stage (i) To learn the reduced-order model, we choose the uniform distribution on $[0, 1]^2$ as the reference $\bar{\rho}$ and compute the Kantorovich potential $\phi(\mu_j)$ that pushes $\bar{\rho}$ to $\rho(\mu_j)$ using the back-and-forth method [19]. Because $\bar{\rho}$ is uniform, the operator \mathcal{L} reduces to the Laplacian, which allows us to compute $\psi(\mu_j) = (I - \mathcal{L})^{1/2} \phi(\mu_j)$ efficiently via the fast Fourier transform. The probability density ρ , the OT potential ϕ , and the transport signature ψ are all represented on $m = n_x^2$ grid points.

We remark that the back-and-forth method solves the unregularized optimal transport problem, in contrast to entropy-regularized approaches such as the Sinkhorn algorithm. Moreover, on regular domains like $[0, 1]^2$, each iteration can be implemented using the fast Fourier transform and elementwise operations, avoiding the need to solve linear systems. Consequently, the method is both accurate and efficient. In our experiment, computing OT potential for $n = 200$ training data takes less than 20 seconds.

Offline stage (ii) By collecting the sampled grid-based transport signatures, we form the finite matrix $\Psi \in \mathbb{R}^{n \times m}$. Applying the skeleton decomposition (Algorithm 2) to $\Psi \Psi^\top$, we select row indices $I = \{i_1, \dots, i_r\}$ with $r = 10$ and form the basis matrix $\Psi_I \in \mathbb{R}^{r \times m}$. The coefficients $a_m(\mu_j)$ and the mapping \hat{a} are learned as stated in Sec. 3.2. The coefficients $a_m(\mu_j)$ are computed by least squares, and the mapping \hat{a} is represented by a neural network with two hidden layers of width 32 and ReLU activations. The neural network is trained by regression using the Adam optimizer with a learning rate of 10^{-3} for 3000 epochs.

We use skeleton decomposition instead of singular value decomposition because it selects representative signatures from the data rather than forming global linear combinations of all snapshots. The resulting basis functions are therefore interpretable as transport signatures associated with actual parameter values. In addition, when the Gram matrix G_m is well

conditioned, the corresponding least-squares coefficient map is stable, which facilitates the subsequent regression step.

In skeleton decomposition, using a larger r improves the low-rank approximation, but it increases the condition number of the Gram matrix G_m , degrades the stability of the coefficient map a_m . The choice of r must balance the low-rank approximation error and the stability of the coefficient map a .

Online stage The online stage is implemented as described in Sec. 3.3. Analogous to the implementation of $(I - \mathcal{L})^{1/2}$ in offline stage (i), $(I - \mathcal{L})^{-1/2}$ is computed using the fast Fourier transform. To compute the pushforward, we obtain $\nabla\phi$ via centered finite differences of a bilinear interpolant of ϕ , and approximate the pushforward integral by adaptive midpoint sampling within each source cell followed by bilinear deposition onto the target grid.

5.2 Verification of low-rank structure

For each parameter μ_j , $j = 1, \dots, n$, the full-order model and offline stage (i) produce $\rho(\mu_j)$, $\phi(\mu_j)$ and $\psi(\mu_j)$, each defined on $m = n_x^2$ grid points. Collecting these values yields matrices of size $n \times m$ for ρ , ϕ , and ψ , respectively. We then compute the reduced SVD to obtain the leading singular values $\sigma_1, \dots, \sigma_{50}$ for the three matrices. We plot σ_i/σ_1 in Figure 2. Figure 2 shows that the leading rank-decay structure of the Kantorovich potential ϕ and transport signature ψ is improved compared to ρ . The ratios σ_{10}/σ_1 for the ϕ - and ψ -matrices are smaller than 10^{-2} , while that of the ρ -matrix is greater than 10^{-2} .

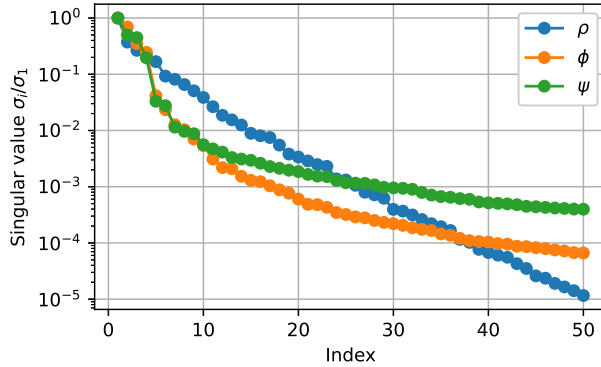


Figure 2: Singular value decay pattern of probability density ρ , OT potential ϕ and transport signature ψ .

5.3 Evaluation of reduced-order model

We evaluate the reduced-order model on three data sets. For each dataset, we compute the Wasserstein-2 distance between the ROM and FOM results $W_2(\rho(\mu), \hat{\rho}(\mu))$ and report the average W_2 distance. We also plot the FOM results (top rows) and ROM results (bottom rows) of 10 sampled or representative snapshots for visual comparison.

1. **Training data:** $n = 200$ snapshots used to train the ROM. The average W_2 error is 0.0214. Figure 3 shows 10 random samples.
2. **Testing data:** 800 snapshots from the same parameter range but not used during training. The average W_2 error is 0.0231. Figure 4 displays 10 random samples.
3. **Unseen parameters:** A newly sampled parameter pair (α, β) evaluated on the same grid ($n_x = n_t = 100$). The average W_2 error is 0.0214. Figure 5 presents the location of the sampled parameter relative to the training set, the corresponding W_2 error evolution in time, and the snapshots $\rho(\mu)$ at $t = 0.1, 0.2, \dots, 1$.

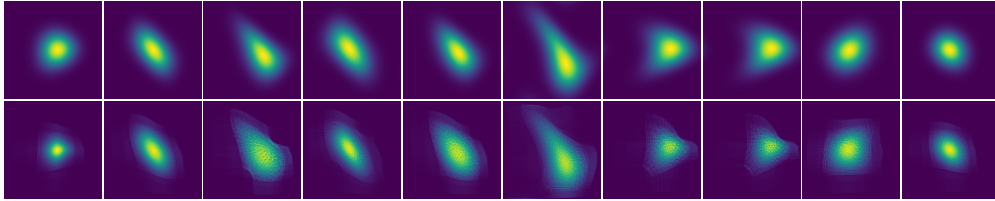


Figure 3: Samples of training data. Top row: FOM results; bottom row: ROM results.

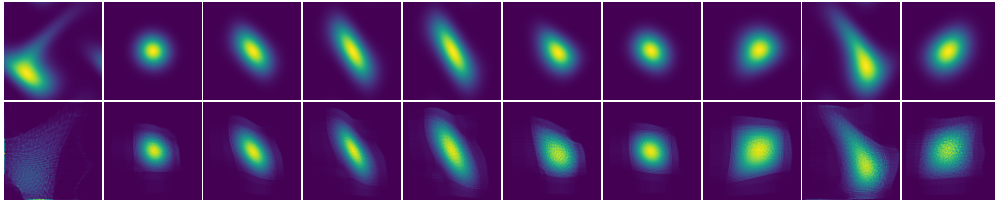


Figure 4: Samples of testing data. Top row: FOM results; bottom row: ROM results.

6 Conclusions

In this work, we introduced an optimal-transport-based reduced-order modeling framework for parametrized density-valued PDEs. For transport-dominated probability distributions, it is more effective to approximate how mass moves from a reference state than to approximate the densities themselves. The skeleton decomposition provides a compact set of representative transport modes, while the learned coefficient map gives a practical non-intrusive surrogate for new parameter values. The accompanying error analysis justifies this construction by linking the approximation error in signature space to the Wasserstein distance between the reconstructed distributions. The numerical experiments indicate that this representation can be effective for the solution of continuity equations. Important directions for future work include improving the choice of reference density, developing adaptive or local reference strategies for strongly multimodal dynamics, and extending the computational framework to higher-dimensional problems where optimal transport calculations are more demanding.

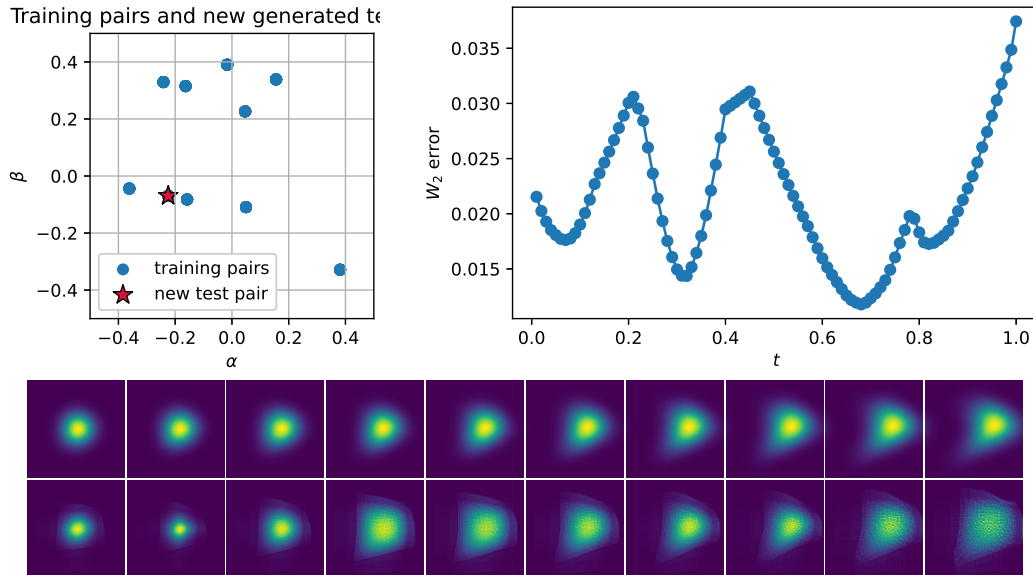


Figure 5: Numerical results for new parameters. Top left: training parameters and the newly sampled parameter. Top right: W_2 error versus t for the new sample. Bottom: $\rho(\mu)$ of an unseen parameter (α, β) at $t = 0.1, t = 0.2, \dots, 1.0$ (left to right) by FOM (top row) and ROM (bottom row).

Acknowledgment

All the authors acknowledge the support of the ICERM workshop “Empowering a Diverse Computational Mathematics Research Community” on July 22 - August 2, 2024, where this work was initiated.

JH is partially supported by National Science Foundation under Grant No. DMS-2409858. FL is partially supported by Air Force Office of Scientific Research under Grant No. FA9550-26-1-0003. ST is partially supported by National Science Foundation under Grant No. DMS-2529292. YY is partially supported by National Science Foundation under Grant No. DMS-2409855 and Office of Naval Research under Award No. N00014-24-1-2088. ZS is partially supported by SIAM Postdoctoral Support Program.

References

- [1] Kenneth Allen, Ming-Jun Lai, and Zhaiming Shen. Maximal volume matrix cross approximation for image compression and least squares solution. *Advances in Computational Mathematics*, 50(5):102, 2024.
- [2] Luigi Ambrosio, Nicola Gigli, and Giuseppe Savare. *Gradient flows*. Lectures in Mathematics. ETH Zürich. Birkhauser Verlag AG, Basel, Switzerland, 2 edition, December 2008.
- [3] Beatrice Battisti, Tobias Blickhan, Guillaume Enchéry, Virginie Ehrlacher, Damiano

- Lombardi, and Olga Mula. Wasserstein model reduction approach for parametrized flow problems in porous media. *ESAIM: Proceedings and Surveys*, 73:28–47, 2023.
- [4] Peter Benner, Albert Cohen, Mario Ohlberger, and Karen Willcox, editors. *Model Reduction and Approximation: Theory and Algorithms*, volume 15 of *Computational Science and Engineering*. Society for Industrial and Applied Mathematics, Philadelphia, PA, 2017.
- [5] F. Bernard, A. Iollo, and S. Riffaud. Reduced-order model for the BGK equation based on POD and optimal transport. *Journal of Computational Physics*, 373:545–570, 2018.
- [6] Tobias Blickhan. A registration method for reduced basis problems using linear optimal transport. *SIAM Journal on Scientific Computing*, 46(5):A3177–A3204, 2024.
- [7] Yann Brenier. Polar factorization and monotone rearrangement of vector-valued functions. *Communications on pure and applied mathematics*, 44(4):375–417, 1991.
- [8] Minshuo Chen, Haoming Jiang, Wenjing Liao, and Tuo Zhao. Nonparametric regression on low-dimensional manifolds using deep ReLU networks: Function approximation and statistical recovery. *Information and Inference: A Journal of the IMA*, 11(4):1203–1253, 2022.
- [9] Wolfgang Dahmen, Christian Plesken, and Gerrit Welper. Double greedy algorithms: Reduced basis methods for transport dominated problems. *ESAIM: Mathematical Modelling and Numerical Analysis*, 48(3):623–663, 2014.
- [10] Minh-Hieu Do, Jean Feydy, and Olga Mula. Sparse wasserstein barycenters and application to reduced order modeling. *Journal of Scientific Computing*, 102:64, 2025.
- [11] Virginie Ehrlicher, Damiano Lombardi, Olga Mula, and François-Xavier Vialard. Non-linear model reduction on metric spaces. application to one-dimensional conservative PDEs in Wasserstein spaces. *ESAIM: Mathematical Modelling and Numerical Analysis*, 54(6):2159–2197, 2020.
- [12] Stefania Fresca, Luca Dedè, and Andrea Manzoni. A comprehensive deep learning-based approach to reduced order modeling of nonlinear time-dependent parametrized PDEs. *Journal of Scientific Computing*, 87(2):61, 2021.
- [13] Sergei A. Goreinov, Ivan V. Oseledets, Dimitry V. Savostyanov, Eugene E. Tyrtyshnikov, and Nikolay L. Zamarashkin. How to find a good submatrix. In *Matrix Methods: Theory, Algorithms and Applications: Dedicated to the Memory of Gene Golub*, pages 247–256. World Scientific, 2010.
- [14] Sergei A. Goreinov and Eugene E. Tyrtyshnikov. The maximal-volume concept in approximation by low-rank matrices. *Contemporary Mathematics*, 268:47–51, 2001.
- [15] Sergei A. Goreinov, Eugene E. Tyrtyshnikov, and Nickolai L. Zamarashkin. A theory of pseudoskeleton approximations. *Linear Algebra and its Applications*, 261(1-3):1–21, 1997.

- [16] Jan S. Hesthaven, Cecilia Pagliantini, and Gianluigi Rozza. Reduced basis methods for time-dependent problems. *Acta Numerica*, 31:265–345, 2022.
- [17] Jan S Hesthaven, Benjamin Peherstorfer, and Benjamin Unger. Nonlinear model reduction for transport-dominated problems. *arXiv preprint arXiv:2602.01397*, 2026.
- [18] Jan S. Hesthaven, Gianluigi Rozza, and Benjamin Stamm. *Certified Reduced Basis Methods for Parametrized Partial Differential Equations*. SpringerBriefs in Mathematics. Springer, Cham, 2016.
- [19] Matt Jacobs and Flavien Léger. A fast approach to optimal transport: the back-and-forth method. *Numerische Mathematik*, 146(3):513–544, 2020.
- [20] Richard Jordan, David Kinderlehrer, and Felix Otto. The variational formulation of the Fokker–Planck equation. *SIAM Journal on Mathematical Analysis*, 29(1):1–17, 1998.
- [21] Moaad Khamlich, Federico Pichi, Michele Girfoglio, Annalisa Quaini, and Gianluigi Rozza. Optimal transport-based displacement interpolation with data augmentation for reduced order modeling of nonlinear dynamical systems. *Journal of Computational Physics*, 531:113938, 2025.
- [22] Soheil Kolouri, Se Rim Park, Matthew Thorpe, Dejan Slepčev, and Gustavo K. Rohde. Optimal mass transport: Signal processing and machine-learning applications. *IEEE Signal Processing Magazine*, 34(4):43–59, 2017.
- [23] Soheil Kolouri, Akif B. Tosun, John A. Ozolek, and Gustavo K. Rohde. A continuous linear optimal transport approach for pattern analysis in image datasets. *Pattern Recognition*, 51:453–462, 2016.
- [24] Quentin Mérigot, Alex Delalande, and Frédéric Chazal. Quantitative stability of optimal transport maps and linearization of the 2-wasserstein space. In *Proceedings of the Twenty Third International Conference on Artificial Intelligence and Statistics*, volume 108 of *Proceedings of Machine Learning Research*, pages 3186–3196. PMLR, 2020.
- [25] Monica Nonino, Francesco Ballarin, Gianluigi Rozza, and Yvon Maday. A reduced basis method by means of transport maps for a fluid–structure interaction problem with slowly decaying kolmogorov n -width. *Advances in Computational Science and Engineering*, 1(1):36–58, 2023.
- [26] Benjamin Peherstorfer. Model reduction for transport-dominated problems via on-line adaptive bases and adaptive sampling. *SIAM Journal on Scientific Computing*, 42(5):A2803–A2836, 2020.
- [27] Gabriel Peyré and Marco Cuturi. Computational optimal transport. *Foundations and Trends in Machine Learning*, 11(5–6):355–607, 2019.
- [28] Donsub Rim, Benjamin Peherstorfer, and Kyle T. Mandli. Manifold approximations via transported subspaces: Model reduction for transport-dominated problems. *SIAM Journal on Scientific Computing*, 45(1):A170–A199, 2023.

- [29] Filippo Santambrogio. *Optimal Transport for Applied Mathematicians: Calculus of Variations, PDEs, and Modeling*, volume 87 of *Progress in Nonlinear Differential Equations and Their Applications*. Birkhäuser, Cham, 2015.
- [30] Alex Townsend and Lloyd N. Trefethen. Continuous analogues of matrix factorizations. *Proceedings of the Royal Society A: Mathematical, Physical and Engineering Sciences*, 471(2173):20140585, 2015.
- [31] Cédric Villani. *Topics in Optimal Transportation*, volume 58 of *Graduate Studies in Mathematics*. American Mathematical Society, Providence, RI, 2003.
- [32] Wei Wang, Dejan Slepčev, Saurav Basu, John A. Ozolek, and Gustavo K. Rohde. A linear optimal transportation framework for quantifying and visualizing variations in sets of images. *International Journal of Computer Vision*, 101(2):254–269, 2013.